NASA/DLR Challenge 2020
Mercurius Aircraft Concept

Team
Cornelius Kauffmann
Jan Rudzki
Manuel Prinz
Nathanael Pfanner
Markus Sailer
Moritz Wenzel

Academic Support and Advisors
Prof. Dr.-Ing. Manfred Hajek
M.Sc. Nicolas André
M.Sc. Florian Berghammer

Institute of Helicopter Technology
Technical University of Munich

Submitted on July 15th, 2020

Team Members

Cornelius Kauffmann, Team Lead
Bachelor Student: Mechanical Engineering
6th semester
Aerodynamics, Propulsion System, Business Case

Jan Rudzki
Bachelor Student: Mechanical Engineering
6th semester
Model Development, Aircraft Sizing, Business Case

Manuel Prinz
Bachelor Student: Mechanical Engineering
6th semester
CAD, Ground Station and Logistic Support, Safety Analysis, Regulatory Affairs

Nathanael Pfanner
Bachelor Student: Mechanical Engineering
6th semester
Market Analysis, Noise Emissions, Mission Profile, Business Case

Markus Sailer
Bachelor Student: Mechanical Engineering
6th semester
Aircraft Systems, Autonomous Operations, Regulatory Affairs

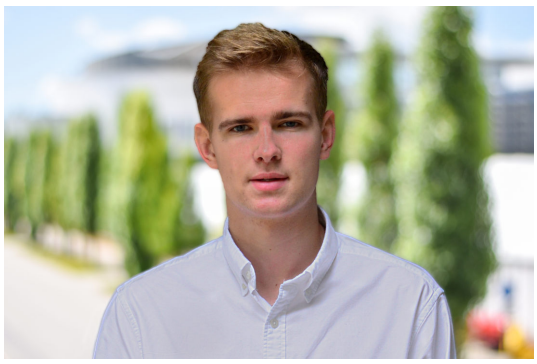

Moritz Wenzel
Bachelor Student: Mechanical Engineering
6th semester
Model Development, Aircraft Configuration Design, Analysis and Performance

Abstract

The continually growing parcel shipping market and the increasing demand for instant delivery force the implementation of new technical solutions. The Mercurius Drone presented in this paper provides one possible solution within the NASA-DLR Design Challenge 2020. The design focuses on maximum efficiency at minimum weight. Two fixed front propellers and six rear tilting top-wing propellers combine the conflicting requirements of high hovering efficiency and efficient cruise behaviour. Design features like downwarded winglets or top-wing props lead to a maximum L/D ratio of over 6 despite low Reynolds numbers, while other concepts (e.g. Amazon) end up with estimated values of 3 [1]. The Mercurius hybrid fuel cell propulsion system enables mission ranges that are unattainable for battery-powered concepts. Additionally, it maximizes flight safety and leads to 30% lower costs per package delivered through more efficient utilization. The productive use of the drone is inseparably linked to the design of the ground unit. The Mercurius ground station (see simulation video in appendix) thus embodies the maximum productivity at minimum cost design philosophy. This allows the required departure interval of 120s to be exceeded and enables dynamic handling. The design of the Mercurius Drone is based entirely on state-of-the-art technology. Thus, such concept could revolutionize conventional parcel delivery.

Technische Universität München | Lehrstuhl für Hubshraubertechnologie
Boltzmannstraße 15 | 85748 Garching
Lehrstuhl für Hubschraubertechnologie
Fakultät für Luftfahrt, Raumfahrt und Geodäsie
Technische Universität München
Boltzmannstraße15
85748 Garching bei München

Garching bei München, 8. Juli 2020

Bestätigungsschreiben

Sehr geehrte Damen und Herren,

Hiermit bestätige ich, dass die Projektgruppe *Mercurius*, bestehend aus den Studierenden

- Cornelius Kauffmann
- Nathanael Pfanner
- Manuel Prinz
- Jan Rudzki
- Markus Sailer
- Moritz Wenzel

die Arbeiten zum Wettbewerb der *Joint NASA / DLR Aeronautics Design Challenge 2020* selbstständig durchgeführt hat. Der Bericht wurde seitens des Lehrstuhls geprüft und genehmigt.

Bei weiteren Fragen wenden Sie sich jederzeit gerne an mich oder an die betreuenden wissenschaftlichen Mitarbeiter:

- Herrn Nicolas André (nicolas.andre@tum.de) und
- Herrn Florian Berghammer (flo.berghammer@tum.de)

Mit freundlichen Grüßen

Prof. Dr.-Ing. M. Hajek

Lehrstuhl für Hubschraubertechnologie
Prof. Dr.-Ing. Manfred Hajek
Technische Universität München
Boltzmannstraße 15
85748 Garching
Tel. 089/289-16353

Contents

Acronyms

ANC	Active Noise Control
BVLOS	Beyond Visual Line Of Sight Operation
CG	Center of Gravity
DAA	Detect and Avoid
DAIDALUS	Detect and Avoid Alerting Logic for Unmanned Systems
DEP	Distributed Electric Propulsion
DGM	Design Gross Mass
DOE	U.S. Department of Energy
EASA	European Union Aviation Safety Agency
EFPA	Equivalent Flat Plate Area
FAA	Federal Aviation Administration
GAN	Generative Adversarial Networks
GNSS	Global Navigation Satellite System
HOD	Hook On Device
ICAROUS	Independent Configurable Architecture for Reliable Operations of Unmanned Systems
IMU	Inertial Measurement Unit
MTBF	Mean Time Between Failures
MTOW	Maximum Takeoff Weight
PDU	Power Distribution Unit
PEMFC	Proton Exchange Fuel Cell
PL	Power Loading
PRD	Pressure Relief Device
RPM	Rounds per Minute
SA	Sensitivity Analysis
SAIL	Specific Assurance and Integrity Level
SPL	Sound Pressure Level
UAV	Unmanned Aerial Vehicle
USB	Upper Surface Blowing
UTM	Unmanned Aircraft System Traffic Management
VO	Visual Operator
VSLAM	Visual Simultaneous Localization and Mapping

List of Figures

List of Tables

1. Introduction

1.1. Market Analysis

Parcel shipping continues to grow, reached $87 billion in 2018 in volume globally, and will hit the $200 billion benchmark in 2025 [2]. However, this development does not remain without consequences. As an example, between Britain, Germany, and the United States, the economic consequences of traffic congestion amount to $461 billion in 2017, or equal to $975 per person [3]. A promising and innovative option is to lift existing traffic into the airspace. Drone delivery could reduce traffic congestion and subsequently reduce associated greenhouse gas emissions [4]. This vision is more relevant than ever. According to the National Aeronautical Centre, 42% of logistics carriers plan to use UAVs in the future [5]. Further, an outlook study by SESAR estimates 100,000 delivery drones in Europe by 2050 [6].

According to McKinsey & Company, last-mile delivery is the most promising application for drone delivery [7]. One primary reason for this is that today's delivery model inefficient, and therefore 53% of the total shipping costs are attributed to this segment [8]. The new approach promises improvements in terms of time, flexibility, reliability, and price, which is especially beneficial for same day, strict time window, or instant delivery.

The aim of the NASA/DLR Aeronautics Design Challange 2020 is to design a small delivery drone within a maximum payload of 2.5 kg and dimensions of 15 cm x 15 cm x 15 cm [9]. Not all parcels fulfill these requirements. As a reference, 86 percent of Amazon's packages weight under 2.3 kg [10]. However, even if they do not surpass the maximum parcel weight, only 70 percent of these parcels are appropriated for drone delivery due to safety and dimension concerns [11].

A predicted market volume of autonomous last-mile deliveries of almost $92 billion in 2030 arouses cross-domain awareness [12]. Unsurprisingly, Unmanned Aerial Vehicle (UAV) development is not the only effort being made to address the enormous demand for last-mile delivery. Competing technologies like autonomous vehicles called droids could achieve a market share of 80% [7]. Therefore it is advisable for a initial market entry to target a specific market where customers are willing to pay a little more. Already today, almost 25% of consumers are willing to pay significantly more for same-day or instant delivery, which therefore represents the perfect customers [7]. Establishing drone delivery services will however be challenging and many hurdles like certification and a broad acceptance in the society have to be overcome beforehand.

1.2. Requirements Breakdown

An efficient design process urgently needs clearly defined requirements. Therefore, the most important requirements are precisely specified in advance. A clear definition of different requirement domains helps to maximize the solution space for the design phase.

Aerodynamic Efficiency A major technical difficulty is the compatibility of aerodynamic efficiency and payload in parcel drone systems. Many concepts carry cargo under the fuselage and thus suffer from high losses in the L/D ratio. An optimization of the glide ratio is particularly important here, since scaling to smaller sizes and speeds results in a shift to smaller Reynolds numbers. This leads to a dominance of friction forces, which worsens the lift at increasing drag compared to large aircrafts [13].

Economic Efficiency The operation of a delivery service using parcel drones can only be introduced on a large scale if the economic benefit is clearly given. The required departure interval of 120 seconds needs a highly efficient utilisation of the aircraft. The charging time of drones directly related to the number of required aircraft in service, which is shown in Figure 1. With shorter departure intervals, the number of necessary drones increases considerably. Since the costs for procurement, maintenance and insurance increase with the number of aircraft, the reduction of ground time to a minimum is a key goal of technical implementation. As a stopover at the base to pick up another parcel can be much faster than refuelling, the number of flyable missions per refuelling cycle should also be increased.

Safety In order to obtain certification by aviation authorities Federal Aviation Administration (FAA) and European Union Aviation Safety Agency (EASA), high requirements for the safety of people and the environment must be ensured. This can be done in two ways. Firstly, the probability of a total failure must be reduced to a minimum. One way to achieve this is to create redundancies in sensors and the powertrain. Secondly, in the event of a total failure, the resulting damage to people and the environment must be minimized. For this purpose, a safety system should be selected, which will take effect in this case.

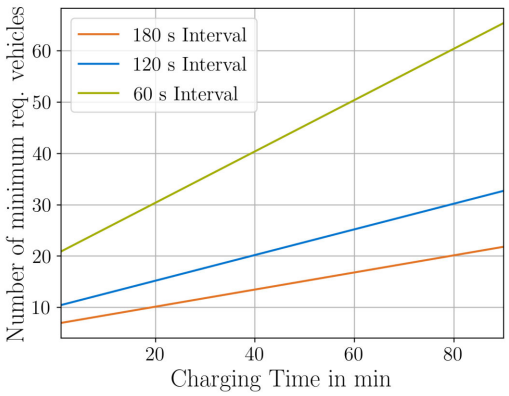

Figure 1: Required number of aircraft as a function of charging time

Noise reduction Even if all the above-mentioned hurdles have been overcome, the introduction of delivery drones requires broad acceptance among the population. One of the most critical factors for this is the operation within acceptable noise levels. Therefore, in addition to the noise level, the frequency range must also be carefully selected in the design, since the human ear perceives high frequencies as louder than low frequencies [14]. The further aim should be to minimize the duration of noise exposure. This can be achieved by short hover times during take-off and landing.

2. Concept Selection

2.1. Methodology

The design phase of a delivery system with drones involves distinct engineering techniques. A systems engineering approach presented in [15] therefore helps to coordinate them effectively. This procedure ensures that all requirements are met and guarantees an accurate adaptation of all subsystems. Initially, a market analysis helps to achieve a broad overview of current development in terms of delivery drones and identifies possible potentials and obstacles. These considerations lead to a first selection of drone layouts, whereby each design decision grounds on a scientific basis. Another important decision is the selection of a suitable energy carrier for the drone. Since there are many options, a cost-benefit evaluates them on weight, efficiency, failure tolerance, cost efficiency, environmental impact, mission applicability and technology readiness.

The applied design methodology extends the conceptual design approach presented by Torenbeek [16], by adapting the procedure to special requirements of small VTOL aircraft. The high complexity of the propulsion system and the drone's unconventional design require new methods that augment the formulas in traditional aircraft design. Therefore a system of parametric models has been developed that enables a quantitative evaluation of the drone layouts. Implementing empirical and quasi-analytical formulas known from current research, the system of models helps to finalize and optimize a specific drone concept. This method allows us to optimize multiple parameters simultaneously and hence to improve the quality of the initial drone layout with every iteration. The rapid development of new technologies leads to uncertainties within the model's input parameters. Therefore an optimistic and a pessimistic case is considered in addition to the baseline value of a particular parameter. The system of models also includes a drone fleet model, which calculates the required number or drones, depending on their performance. It helps to set the requirements for the drone in such a way that an overall economical concept is created. Finally, the fulfillment of all requirements and design goals is verified.

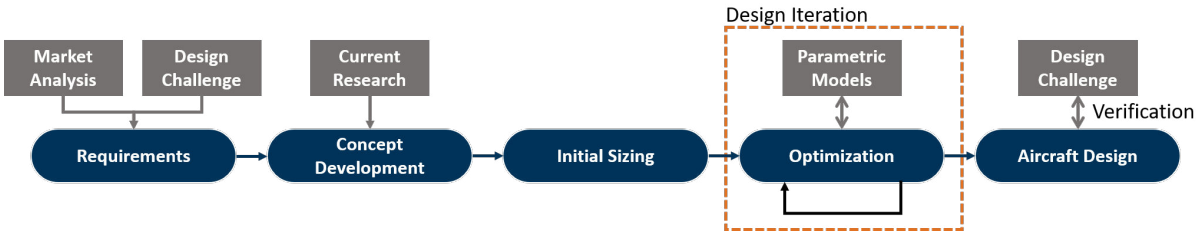

Figure 2: Visualization of the Design Method

2.2. Parametric Model

Figure 3 shows a flow chart of the corresponding parametric models used to acquire the drone's specifications. Initially, the UAV Sizing Model provides a basic estimation of the drone's Design Gross Mass (DGM) with the input of an assumed aerodynamic efficiency and mission parameters, that are given by the task. In the next step, the initial dimensions and specifications of a preliminary aircraft design are fed to further models that calculate precise aerodynamic parameters. Additionally, a sensitivity analysis for the Sizing Model's input parameters is carried out in order to assess which criteria require special attention in the further procedure. Although the CAD model has been continuously improved in parallel to the optimization of the drone concept, CFD analysis is not used, since the application of these methods requires prior knowledge and can quickly produce incorrect results [17]. Instead, an Aerodynamic Drag Model, according to [17] that yields the Equivalent Flat Plate Area (EFPA) of an aircraft is implemented and integrated into the overall Aircraft Model.

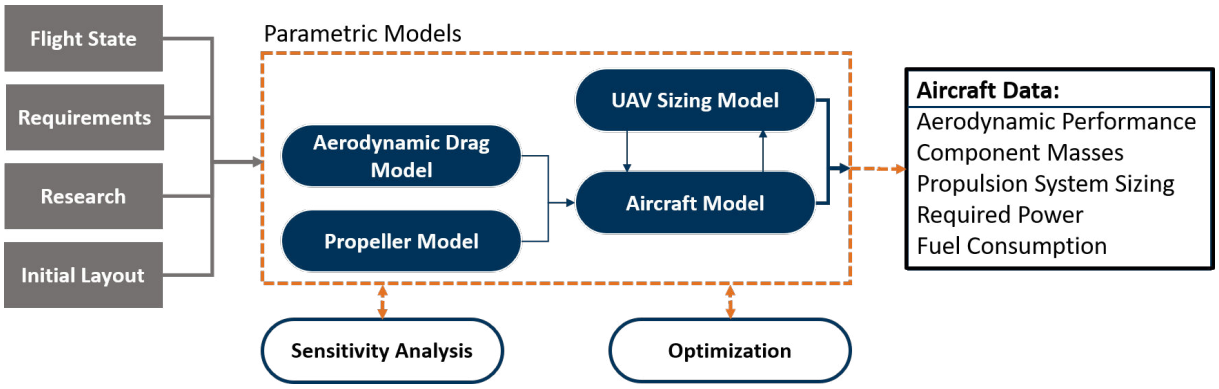

Figure 3: Corresponding Models

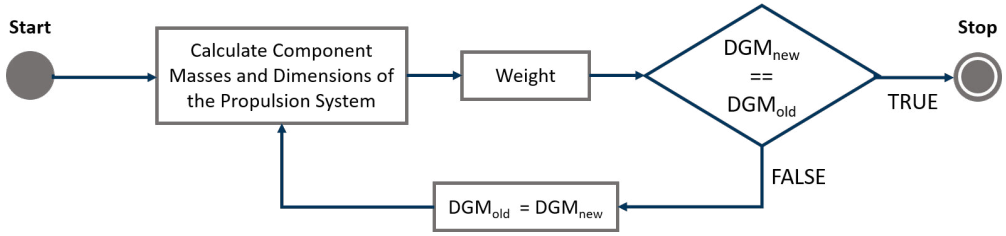

Figure 4: Block Diagram of the Sizing Algorithm

Iterative Component Sizing with UAV Sizing Model The algorithm is used to size the delivery drone and its components to a given set of input parameters. These are mission specifications such as cruise range and hover time, the drone's aerodynamic performance calculated with the Aircraft Model and other values that characterize the propulsion system. The structural weight is calculated as 40% of the DGM. Initially, the algorithm estimates a starting value for DGM. In the following iterations, it minimizes the DGM and matches the mass of all aircraft components exactly to the dimensioning of the propulsion system.

Aircraft Model The aircraft model performs a stationary Trim for every flight state of the flight envelope to get the aircraft data (power requirements, drive and tilt of the rotors). A component build-up method is used. For each component (fuselage, rotors, wings), the resulting forces and moments are calculated and added to the Trim equation system. The equation system is solved by adjusting the control factors like the orientation angles. The rotors are modeled by momentum theory [18], and the results are verified by a blade element theory tool [19]. The wings are modeled by aerodynamic coefficients from empirical data (NACA23012) and the aerodynamic drag model. According to Wirth [20], a model of this fidelity provides almost the same information value as more detailed and complex models. Linking the aircraft model with the sizing model helps to optimize the drone layout and ultimately provides essential parameters such as DGM, aerodynamic efficiency, and energy consumption.

3. Aircraft Design

3.1. Aircraft Configuration

The design of the Mercurius Drone focuses on high aerodynamic efficiency combined with minimal weight. A lift-generating body together with slender lifting surfaces, a hybrid fuel cell and battery powered propulsion provide a high lift-over-drag ratio, high specific energy and high specific power of the overall system. This chapter presents the most important design decisions of the concept and finally validates the overall concept.

Figure 5: Aircraft Design

Wing Configuration The chosen configuration with a slender wing and a front canard connects the propeller mountings to the wing surface. This avoids any additional structure to the propeller mounting, which would lead to parasitic drag increase and weight increment. Implementing a front canard involves the risk of an unstable flight attitude. To avoid this, it must be ensured that the aerodynamic center of the configuration remains behind the center of gravity, which is located next to the package. This is achieved by the large rear wing that provides the main lift.

Properties	Value
Wetted Area	1.28 m^2
Wing Area front $S_{ref,f}$	0.05 m^2
Wing Area rear $S_{ref,r}$	0.2 m^2
Span b	1.84 m
Aspect Ratio rear AR	16.2
Taper Ratio λ	0.35

Table 2: Aircraft Properties

Propeller Configuration The Mercurius Drone is provided with thrust from eight propellers, with the two forward canard propellers being slightly tilted and generating lift in all flight states. The six rear propellers are located on the wing surface at 30% chord length and are equipped with a tilt Upper Surface Blowing (USB) mechanism. This arrangement offers several advantages: In [21] the aerodynamic efficiency at different propeller positions was investigated. The authors concluded that positioning two propellers at 30% of the chord length from the wing leading edge improves the L/D ratio by up to 17.6% compared to the clean wing,

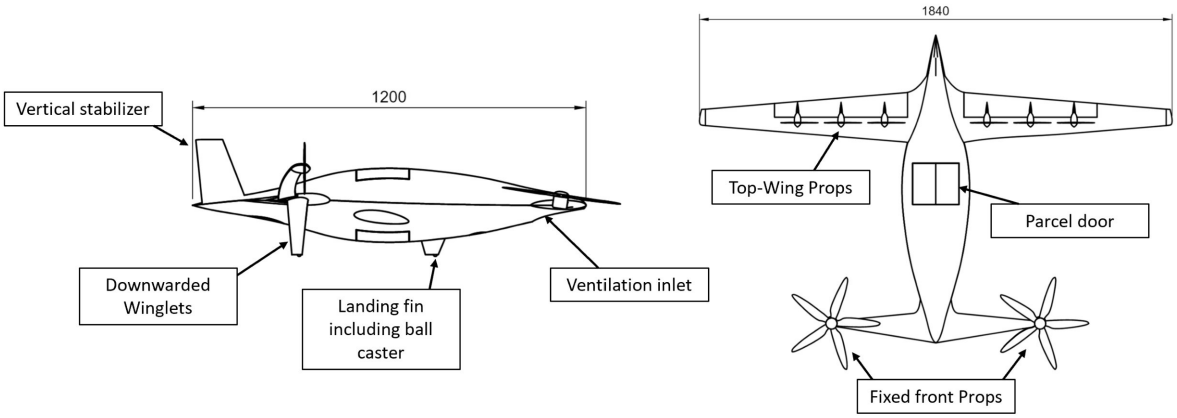

Figure 6: Main design components of the Mercurius Drone

whereby an extension of the number of propellers leads to further improvement (see Figure 7). This effect arises for two reasons.

Firstly, it strengthens the leading edge suction tip in the intake area of the propeller, thus providing additional thrust. Secondly, the propeller on the opposite site increases static and total pressure, which leads to a pushing effect. A placement of the propellers on the wing also offers benefits in the area of noise reduction, which is discussed in more detail in Section 3.5. The rear propeller mountings slope in the flow direction to avoid increments in static pressure at the stagnation points of the structure, which would place asymmetrical load on the blades.
The tilt mechanism of the propellers is combined with the flaps to use the Coanda effect of USB systems. This ensures high lift of the wings even at low speeds, which minimizes the time in the energy inefficient hover. The system is taking advantage of accelerating the airflow on the wing surface and thus shifting the flow separation to higher flap angles. In [22] this effect was investigated and an increase of the $C_{l,max}$ of up to 80% at a flap angle of 20° compared to regular flaps was determined.

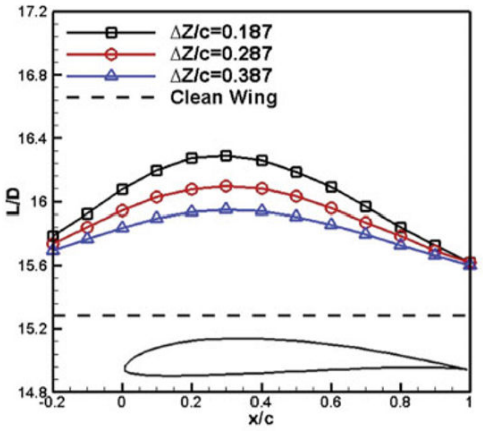

Figure 7: L/D improvement in dependency of position on wing [21]

Since the tilt mechanism must be fully functional at all times, the Mercurius Drone is equipped with two servos for each flap. These are provided with an electrical locking gear so that no electrical load is applied to the servos in stationary operations. The maximum active torques of up to 2.3 Nm can thus be tolerated even if one servo fails, ensuring high redundancy.

Downwarded Winglets A particularly striking design feature of the Mercurius Drone are the downwarded winglets, which are also used as landing legs. As the drone is supposed to fly at high lift and slow speed during take-off and landing, this configuration minimizes the induced drag. Researchers at the University of Toronto showed in 2017 that a downward orientation is more than 80% superior to a conventional upward orientation. When used in a Boeing 737, up to 2% of the total drag could be saved. Compared to winglets oriented upwards, the drag can be reduced because the edge vortex is pushed further outwards in this configuration. If the wing is deformed in flight, the tip of the winglet will be directed outwards, whereas if the winglet is oriented upwards the tip will approach the fuselage. This second effect pushes the wing tip vortex

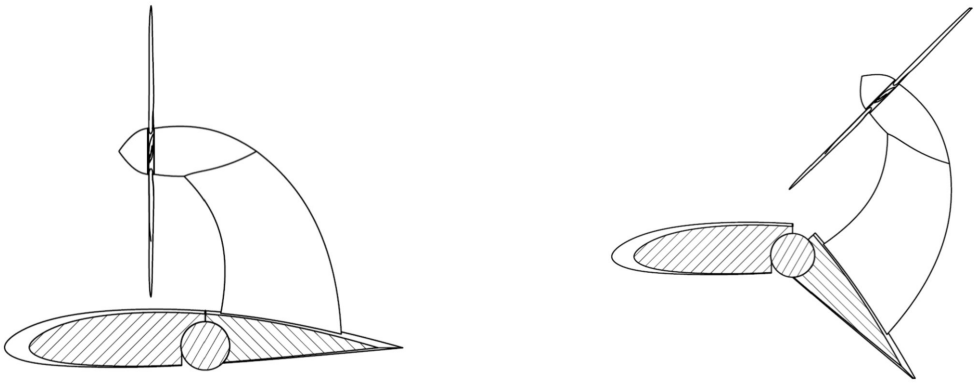

(a) Propeller in horizontal Postion for cruise flight state

(b) Propeller in an angled postion for high lift flight state

Figure 8: Propeller configurations for different flight states

even further outwards.[23] Passenger aircraft find it difficult to take advantage of this technology because they have to maintain required angles around the roll axis during take-off and landing without touching the ground. In the case of a vertical take-off and landing Drone, these restrictions do not apply. Figure 9 shows the transverse force flow and bending moments on the wing in the hover. The winglets at the wingtips lead to a reduction of the wing root bending moment.

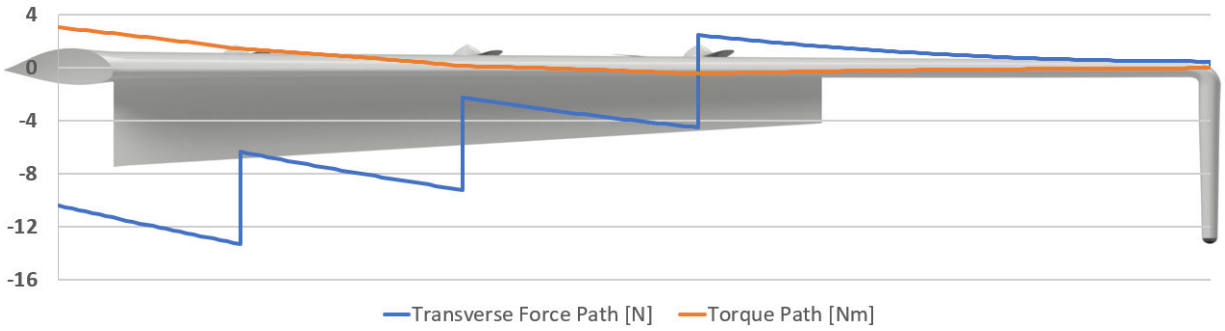

Figure 9: Loads under consideration of the wing weight

Fuselage Design The fuselage design is inspired by bionic shapes found through evolutionary methods like pointed out in [24]. Thus, outstanding drag coefficients $c_D < 0.05$ are possible. The shape can be adopted in a quite similar manner, as Reynolds numbers at a scale of 10^6 appear within the operation scenario. In the Mercurius Drone the parcel is accommodated inside the fuselage, since additional carrying structures used in the "DHL Paketkopter" or the "Wingcopter" do not provide lift, significantly disturb the flow, and therefore lead to an increase of the drag coefficient C_{d0}. In order to enable a simple loading at the same time, opening flaps are installed on the upper and lower sides of the drone. This allows the drone to be loaded from above on the ground, which reduces the complexity of the autonomous ground infrastructure. This point is discussed in more detail in Section 4.1.

3.2. Propulsion System

The Mercurius Drone is supplied with a hybrid propulsion system consisting of a hydrogen-powered fuel cell and a battery. This takes advantage of combining the high energy density of hydrogen and the high power density of lithium ion batteries, resulting in a significant reduction of the DGM [25]. Since the choice of propulsion system has an impact on safety, profitability and energy efficiency in addition to aircraft performance, the design decision could not be made independently of these variables (see Table 3). However,

our analyses show that the short refuelling time of hydrogen tanks and the resulting high efficient utilisation of the aircraft, as well as the increase to three flyable missions result in decisive advantages over a purely battery-powered version (see Chapter 6). Furthermore, the enhanced redundancy of the hybrid version and other aspects offer highest flight safety (see Chapter 5). In this section only the most important technical elements concerning the effects on DGM are discussed, while Table 3 also addresses the findings from the Chapter 5 and 6.

	Battery electric	Fuel Cell electric	Hybrid electric
DGM	-	+	++
Profitability	-	+	+
Energy Efficiency	++	-	-
Safety	-	+	++

Table 3: Propulsion System Comparasion

Sizing Parameters The sizing code presented in Chapter 2 evaluates the aptitude of distinct energy storage methods. Without knowing the exact aerodynamic performance of the drone in the early design stage, sensitivity analysis is used to determine which energy carrier results in the lowest DGM. When choosing the propulsion system, we compare three concepts in terms of their Maximum Takeoff Weight (MTOW) under different Power Loading (PL) and L/D conditions.
Firstly, a propulsion system using Lithium Ion Batteries is investigated. For the calculation we assume a maximum energy density of modern lithium ion batteries [26, 27] of 260 Wh/kg. We divide the energy density by the optimistic value of 1.2 to get the energy density at pack level. Secondly, a system using a hydrogen-powered Proton Exchange Fuel Cell (PEMFC) is investigated. Fuel cell systems offer the potential of high energy densities with short refueling times of less than five minutes and are therefore an attractive comparison partner to the lithium ion battery. One disadvantage of fuel cell systems is the decoupling of power supply and energy storage. A fuel cell stack requires additional weight during short power peaks, while the battery does not need to be enlarged. The Mercurius Drone thus combines the fuel cell with a hybrid battery to be able to deliver high power and energy density. This is evaluated in a third approach. The developed sizing code determines the optimal degree of hybridization of battery and fuel cell to achieve the minimum take-off weight.
The power density of modern PEMFCs has improved dramatically in recent years. Fuel cell cars reached specific power densities of 2.0 kW/kg [28], while in R&D numbers up to 2.23 kW/kg [29] were already achieved in 2017. Since additional mass is required for ventilation and power management, we assume 70% of this value. We also base our tank system on values from the automotive industry, where storage densities up to 7.18 wt.% are achieved at 700 bar storage pressure [30]. Higher gravimetric storage densities can be achieved at 350 bar storage pressure, since the density of hydrogen increases disproportionately with rising pressure [31]. In [32] it was shown that the tank mass could be further reduced by up to 15% with a spherical tank compared to a cylindrical tank. For our calculation we nevertheless assume a storage density of 7 wt.%, since tanks of the size of a parcel drone are produced less frequently and are therefore not optimized as much.

Property	Value	Unit
Lithium Ion Pack specific Energy	217	Wh/kg
Hydrogen grav. Energy Density	33.33	kWh/kg
Fuel Cell specific Power	1.55	kW/kg
Fuel Cell Efficiency	55	%
Fuel Cell Tank System 350 bar Hydrogen Fraction	7	%
Motor Efficiency	85	%

Table 4: Summary of key assumptions for sizing

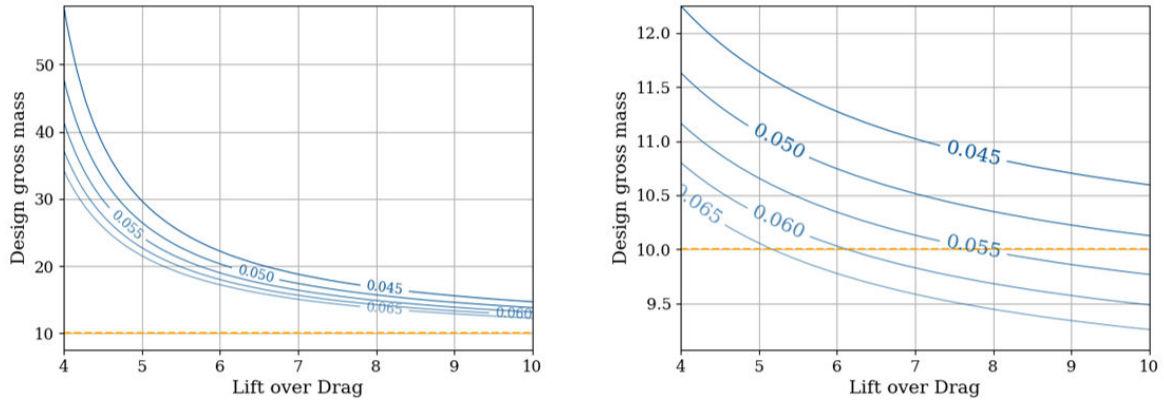

(a) Contour plot of DGM alnong levels of power loading (N/W) and L/D ratio for a battery powered configuration

(b) Contour plot of DGM alnong levels of power loading (N/W) and L/D ratio for a concept, powered by the hybrid propulsion system

Figure 10: Comparison of the DGM of a battery and a fuel cell configuration

Sizing Results Figure 10 shows the results of a sensitivity analysis. The y-axis scaling of the two plots is different and for a better understanding, the orange line marks a DGM of 10 kg in both plots. The battery configuration is more sensitive to L/D and results in higher DGMs. With the hybrid configuration, the lower sensitivity to aerodynamic efficiency results in greater freedom in aerodynamic design. Table 5 summarizes the results of the sizing for a use case with three missions without refueling and the actual aerodynamic parameters. The hybrid configuration achieves the lowest weight of 10.3 kg by combining high gravimetric energy density and high power density. This reduction in Takeoff-Weight also results in a minimal amount of required flight energy and noise emissions.

Concept	Powertrain	Weight (kg)
Mercurius	Hybrid	10.3
Mercurius	Battery	17.26
Quad	Hybrid	12.
Quad	Battery	not converged
Tiltrotor	Hybrid	11.06
Tiltrotor	Battery	25.07

Table 5: Comparasion of different concept weights

3.3. Powertrain and Packaging Concept

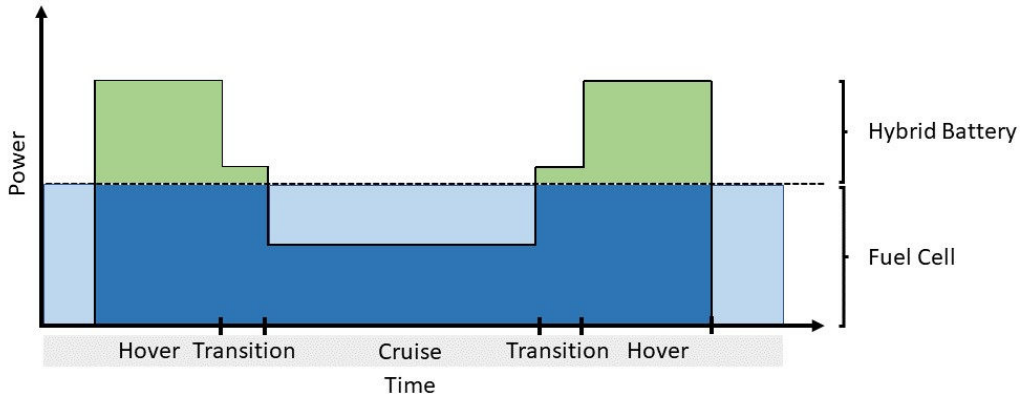

Figure 11: The diagram shows qualitatively the distribution of power for fuel cell and battery. In the light blue areas the battery is charged by the fuel cell.

Powertrain Besides the fuel cell and the 350 bar hydrogen tank, considerably more subsystems are required in a fuel cell system. Those include the ventilation unit, the hybrid battery and a power management system that regulates the performance of the fuel cell and battery [33].

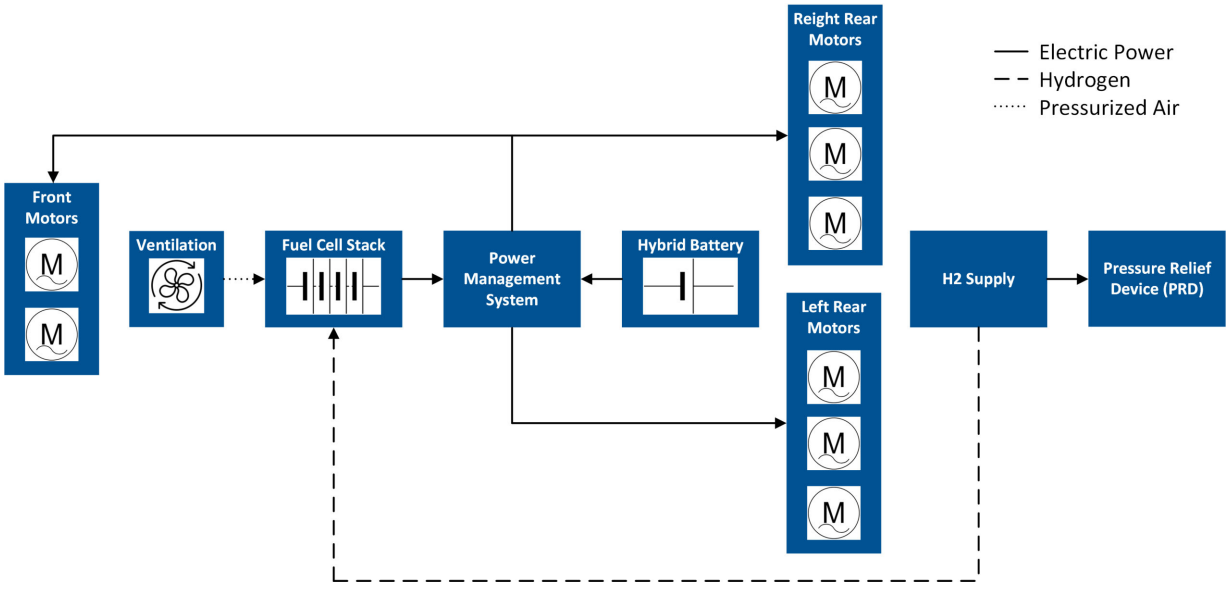

Figure 12: Illustration of the Powertrain (other system components such as controllers or the PDU are not displayed for the sake of simplicity)

The size of the fuel cell and hybrid battery is optimized to achieve a minimum total weight. Due to the significantly higher power density of lithium ion batteries compared to fuel cell stacks, the battery must support the fuel cell in its power output during power peaks such as the hover. The power of the fuel cell must still be sufficient to recharge the battery in the cruise and on the ground. Figure 11 illustrated this dependency.

The sizing model finds the fuel cell power at 920 W. Since the fuel cell is in a small power range, passive cooling is the more weight-optimal and cheaper solution compared to liquid cooling systems [34]. Passive cooling is achieved by coupling the oxygen flow for the reaction with the cooling function and thus replacing a more complex liquid cooling. The system consists of simple propellers that suck air from the air inlet and blow it into the stack at a compressed rate. A power management system (see Figure 12) regulates the power of battery and fuel cell and feeds it via a Power Distribution Unit (PDU) to the individual consumers depending on the power requirements. The hydrogen tank is equipped with a Pressure Relief Device (PRD), through which the hydrogen can be blown off controlled in case of too high pressures in the tank or in emergency situations [35]. Since the hydrogen immediately evaporates and rises upwards due to its low density, neither humans nor the environment are endangered [36, 37].

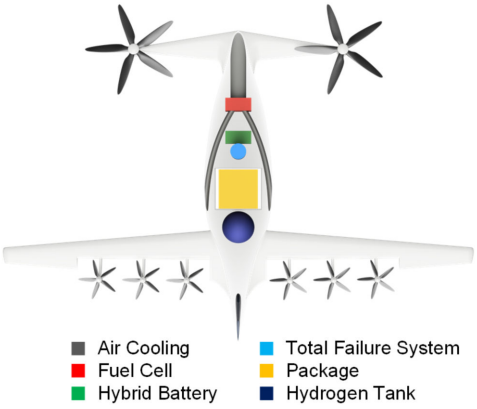

Figure 13: Packaging Concept

Packaging The hybrid fuel cell system requires careful positioning in the Mercurius Drone. The fuel cell is located at the tip of the drone to supply the stack with air through the ventilation inlet at the front bottom of the drone. In this way, the air is used both for cooling and oxygen supply to reduce weight. During flight, the dynamic pressure of the airflow is used to relieve the aerators in their work. The spherical tank geometry blends in well at the rear of the Mercurius drone, which has the advantage of positioning the PRD at the end of the configuration. Refuelling can thus also be carried out easily at the same position. The package

is positioned close to the center of gravity to ensure the same aerodynamic behaviour in both loaded and unloaded flight states. Figure 13 illustrates the individual components in the Mercurius Drone.

3.4. Aircraft Systems

The aircraft is equipped with six cameras with built-in postprocessing capabilities based on a neural network architecture (Deep Learning Cameras [38]) for distance and height measurements, detection of possible collisions and landmark classification (see Section 4.2). Combined with adequate lenses, a field of view of horizontal 80 deg and vertical 50 deg by providing a range of more than 950 m is realistic [39]. In total, five cameras enable a 360 deg horizontal field of view with 40 deg overlap. A vertically installed camera complements the optical system in order to gather additional height information and enable full compatibility with the autonomous logistics system by detecting the correct landing platform. The Mercurius Drone utilises a Active Noise Control (ANC) system to minimize external noise (see Section 3.5). This contains a microphone, a control system and a speaker directed to the ground, which can be easily extended and adapted [40].

A solution with external gimbals was abandoned, so that every component is in an aerodynamically advantageous manner accommodated within the fuselage. Supplementary to the optical system, a Radar system is integrated to face camera issues like pointed out in Section 4.2. Besides Global Navigation Satellite System (GNSS), barometer, optical flow and Radar, an ultrasonic sensor provides height information for distances under 4 m [41]. While being small, light and cost-efficient, a very high measurement accuracy less than 3 mm is achieved [41], enabling a smooth landing with limited stress on payload and structure.

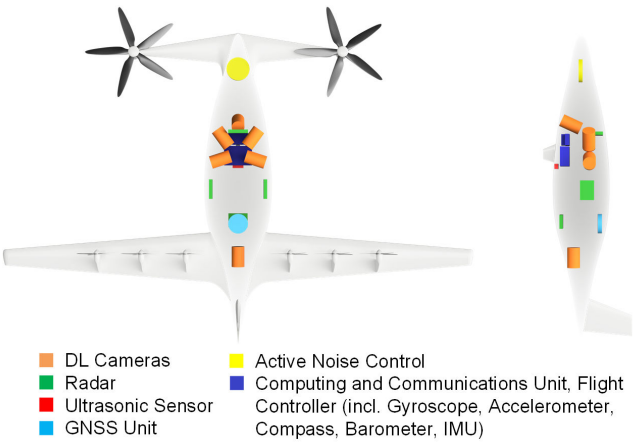

Figure 14: Sensor and Computation Architecture

3.5. Noise Emissions

Parcel drones will operate in more or less densely populated areas wherefore the noise development requires special consideration. The aim is to achieve the lowest possible noise emissions to increase public acceptance on the one hand and to minimize the environmental impact on the other [14]. The focus of noise control should be on operations near ground level since noise level drops down significantly with increasing vehicle altitude (see Figure 15) [1]. Drone noise has mainly three different types of sources [42]. Firstly, the propulsion system within the hybrid powertrain and its eight propellers. Secondly, the vibration of the aircraft structure. And thirdly, the sound of the airflow around the fuselage and wings. Because of the relatively low travel speed compared to other applications, the aspect of airflow is negligible [42].

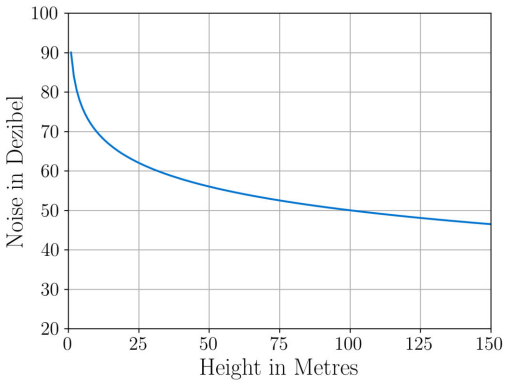

Figure 15: Noise reduction with increasing distance

In the following, we present our noise reduction measures which are divided into passive techniques and active techniques. The advantage of passive techniques is thier mostly easy implementation and present feasibility. Avtive techniques are associated with a high degree of complexity and are preferably installed in larger drones [43]. With future developments and increasing demand, such systems will be used in smaller

drones as well. The following paragraphs outline the passive and active means of noise reduction considered in the Mercurius drone:

Distributed Electric Propulsion (DEP) The Mercurius Drone benefits especially from DEP by using eight individual propellers. Besides redundancy enhancement as described in Chapter 5 and better efficiency Distributed Electric Propulsion (DEP) enables many possibilities in terms of Sound Pressure Level (SPL) improvements [1] or reductions of the blade tip velocity.

Top-Wing Propellers The central positioning of the six rear propellers above the wing does not only affect the efficiency described in Section 3.1. The wings and the fuselage shield a part of the noise towards the ground [44] while cruising. In hover, this effect is not sufficient, as the vehicle operates at low altitude.

Propeller Tip Speed The Mercurius Drone uses DEP and five-bladed propellers to minimize the blade tip speed, as this enters the noise with the fifth to sixth power [14] and is, therefore, one of the primary noise sources. A big advantage of the hybrid configuration is the significant weight saving, which leads to a lower required tip speed in all flight states. Besides this, our set design target of maximum 120 m/s propeller tip speed is achieved by increasing the numbers of all blades up to five, as shown in Figure 16. This enhancement reduces the noise emissions up to 10 dB due to lower tip speeds [43][45].

Propeller Profile The propellers of the Mercurius Drone are equipped with boundary layer trips to further reduce noise. Broadband noise reductions of 6 to 7 dB are achievable due to removing the separation bubble [46]. This promising approach has already been successfully tested at similar scales to our concept [47].

There are many other approaches and studies posing a noise reduction potential of optimized profile shapes from 2 up to 7 dB [46][47] [48][49]. The ideas reach from wavy rotors that pledge 1.4 to 2.0 dB noise reduction for almost all thrust values without significant influence on aerodynamic performance [48], over to special laminates for the propellers like the 'butterfly acoustical skin' [49]. Future studies and testing will help to identify the most appropriate means of noise reduction. These findings can be further incorporated in a later design phase of the Mercurius Drone.

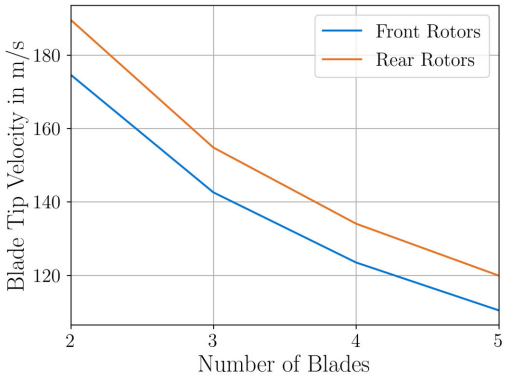

Figure 16: Blade tip speed in relation of the number of blades

Flight Paths The Mercurius Drone's excellent range provides the ability to use intelligent flight path planning to keep noise exposure to humans and the environment to a minimum. A simple but effective approach is the allocation of flight paths next to dense traffic infrastructure. Thus, road traffic noise drowns low- and medium-frequent noise generated by the drone [50].In locations with significantly lower background noise such as parks, rivers, or roads with little traffic, drone noise is perceived more intensely [50]. Therefore, the distance to people can be increased by imposing flight restrictions [51].

Propeller Phase Synchronization Due to a large number of propellers, a propeller phase synchronization control system, as demonstrated with NASA's GL-10 UAV, is adopted in the Mercurius Drone. Slight phase-shifting distributes the sound energy evenly over various harmonics and thus reduces the overall noise level [1]. Predictions on noise reduction are difficult to make as they depend heavily on the observer's location and external effects. However, in [52], a possible 20 dB reduction in the average sound pressure level over a 45-degree range was measured. It is expected to leverage a part of this in real environment.

Active Noise Control (ANC) For the Mercurius drone, we intend the installation of an ANC. This method allows the reduction of annoying noise through the use of destructive interference between an artificial external acoustic signal and the offending noise [53]. As mentioned in Section 3.4, the ANC consists of three components: microphone, control system, and a speaker that are integrated into the drone environment. This applicability has been successfully demonstrated on UAVs and showed particular strengths, especially

at low frequencies [40]. As it is challenging to give exact noise reduction figures that this measure of the Mercurius Drone achieves, the investigation in Figure 17 can be used as an assessment. The authors measure SPL improvements by ANC from 40 up to 80 % in a 30 x 30 m field where the drone flies 20 meters above the ground [40].

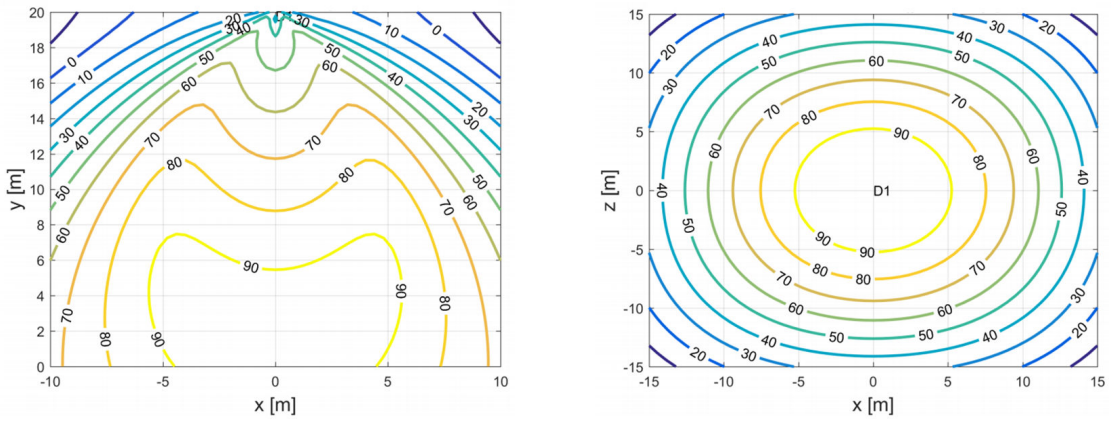

(a) Relative Improvements (z=0 m) [%]

(b) Relative Improvements (y=1.7 m) [%]

Figure 17: Relative SPL improvements by ANC [40]

All in all, there are many possibilities to lower the noise level of the UAV. The interaction of presented measures and its total noise reduction potential requires further work. In order to make a more precise statement, appropriate simulations and real tests are needed.

3.6. Total Failure Compensation

Failure containment of the Mercurious Drone is mandatory. The total failure system enables a controlled emergency landing, even if no other system aboard the drone is active and prevents property damage and, above all, personal injury. For this purpose, a parachute and an airbag are deployed and decelerate the drone to a maximum vertical speed of 2 m/s. Additionally, an acoustic warning signal ensures that people in the landing zone are aware of the sinking drone.

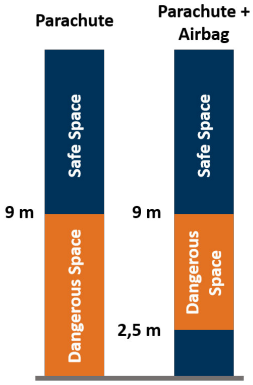

Figure 18: Boundaries of the Total Failure System

Capability According to [54] a drone with these dimensions must be on heights above 9 meters for the parachute to inflate correctly. The resulting dangerous space can be reduced by the use of an airbag [55]. This system is feasible for avoiding any damage if a total failure occurs at a height of less than 2.5 m and guarantees a soft impact after the parachute is deployed [56]. Figure 18 shows that there is still a dangerous space remaining. This does however not pose a risk to humans, as the drone's mission profile stipulates that it climbs up to more than 9 m within the base station's secured area. A total failure at heights between 2,5 m and 9 m would, therefore, only cause material damage.

Activation The total failure system is activated either by the board computer due to a critical failure or by acceleration forces indicating loss of control. These are measured by an independent system, which is directly connected to the parachute deployment device. This system structure ensures that the safety procedure is initiated, even if the board computer is no longer capable of doing so.

Outlook Although the applied total failure system meets all requirements, the advantages of parachutes and airbags could be combined into a single system. The US-Patent [57] of 2017 describes an inflatable cage

that forms around the aircraft due to an uncontrolled condition. The assembly also includes a structure of parachute material, that decelerates the vertical speed until impact. Since this system is not yet available, it cannot be applied to the drone, but it offers a promising basis for the future development of total failure systems.

3.7. Aircraft Performance and Verification

This section examines the overall performance of the Mercurius Drone and ensures that the requirements specified in Section 1.2 are met. The results presented here are the latest state of an iterative design process.

Sizing Mass Table 6 provides a summary of masses and positions of components and the resulting Center of Gravity. As required, the parcel is placed next to the center of gravity. The selection of a hybrid-electric powertrain leads to a significantly lower weight than for a battery-power supply. The efficient aircraft configuration supports this effect. Therefore the DGM of the Mercurius Drone is the lowest for the defined mission requirements (see Table 5).

Component	Weight (g)	Position (cm)
Aircraft Systems	1062	50.1
Battery	74	41.8
Fuel Cell	592	29
Hydrogen Tank	711	77
Electric Motors Front[1] [58]	265	7.6
Electric Motors Rear[1] [59]	489	87.2
Servo Motors	268	89.5
Rotors Front	40	7.4
Rotors Back	120	85.9
Avionics Front	326	6.6
Avionics Rear	1394	87.3
Fuselage	2546	56.4
Payload	2500	62
CG	10387	60.46

Table 6: Weight Breakdown and CG

Property	Value
Span	1.84 m
Length	1.2 m
Height	0.4 m
max. Tip Speed Hover	120 m/s
max. Tip Speed Cruise (42 m/s)	100 m/s
Power Hover	1752.7 W
Power Loading Hover	0.057 N/W
Disk Loading Hover	290.7 N/m^2
Power Cruise	781.04 W
Power Loading Cruise	0.067 N/W
Disk Loading Cruise	149.4 N/m^2
L/D Cruise at 42 m/s	5.4
Figure of Merit	0.635

Table 7: Overview in Standard Atmosphere

Power Requirements As Power Loading and Figure of Merit show, the Mercurius drone is very efficient in hover, and the tip speeds of the rotors are sufficiently low to achieve low noise (see Table 7). The aerodynamic improvements introduced in this chapter result in a maximum L/D ratio of greater than 6 despite low Reynolds numbers, while other concepts (e.g. Amazon) end up with estimated values of 3 [1]. The aerodynamic efficiency is also satisfying the requirements from Section 1.2. Nevertheless, both could be improved, e.g., by optimizing the airfoil profiles of rotor blades and wings with advanced computational tools (see Figures 22 and 31). The power curve in Figure 19a shows that the Mercurius drone usually operates at maximum range speed, rather than at the point of best endurance. Moreover, Figure 19b demonstrates the successful trade-off between the hover efficiency of a quad-concept and the cruise-efficiency of a tiltrotor-concept. This ensures low tip speeds and long-range flights.

Flight Phases and Control Parameters Besides its efficiency, stability and control of the aircraft are crucial. Therefore full control throughout all flight phases is ensured. The flight envelope separates into three main phases. Firstly, the hover phase between 0 and 14 m/s where the rotors mainly produce the thrust. Secondly, a short transition phase between 15 and 17 m/s. In the cruise phase starting at 18 m/s, the wings provide the main lift. Figure 20 gives an impression of the control parameters during different flight phases and transition. Notice that the concept can operate in a steady-state for each point of the envelope. This is

[1] including ESCs [60]

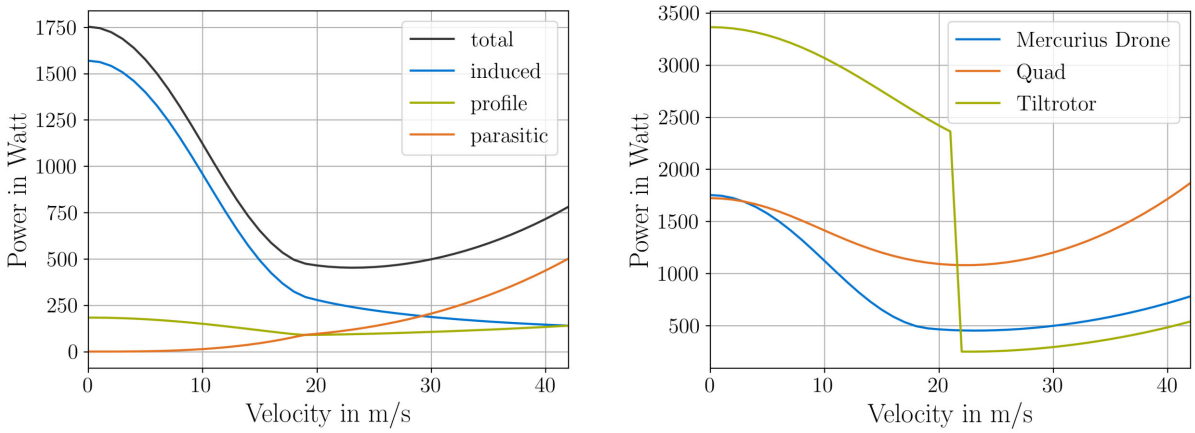

(a) Bath tub curve Mercurius drone

(b) Bathtub curve compared to other concepts

Figure 19: Power requirements of the aircraft concept

enabled by a distinct separation between control parameters for lift, propulsion, and balance of moments. Lift in cruise flight is mainly provided by the main wing and front canards, and controlled by the angle of attack. The rear rotors compensate drag in cruise and provide lift in hover. In forwarding flight, they are fixed in flight direction and controlled only by the Rounds per Minute (RPM). To transit between hover and cruise, the rear rotors are tiltable. In cruise a large part of the front lift is taken over by the candard while the front propellers task shifts to stability control.

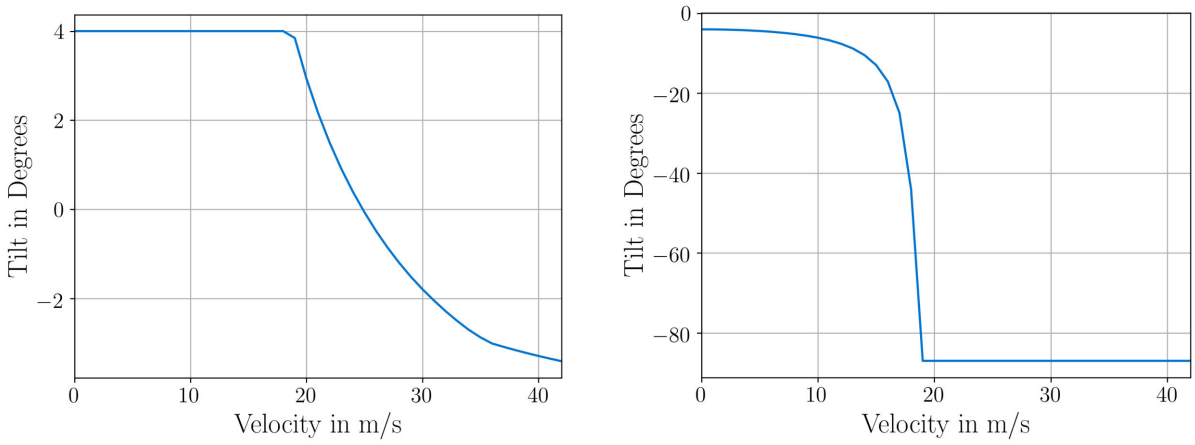

(a) Tilt Angle of Fuselage Across

(b) Tilt Angle of Rear Rotors

Figure 20: Tilt angle of components across flight state

Worst Case Scenario: Hot, High and Head wind To meet the mission requirements of service ceiling at 2500 meters height and 20 knots headwind, we sized the Mercurius drone according to these constraints. The wind adds up to the desired cruise velocity of 113.4 km/h to 151.4 km/h sizing velocity. Figure 21 compares the power requirements in the standard atmosphere (air density: 1.225 kg/m3) and at 2500 meters (air density: 0.95 kg/m3). Hot and High power requirements are higher for almost all phases of flight. Therefore, we chose the higher power requirement at each time to size our drone. As a result of taking the worst-case scenario for sizing, Mercurius drone is capable of higher ranges and cruise velocities than stated in the operation concept and business case sections. The blade tip velocity reaches its maximum in high conditions at 136 m/s in hover.

Verification of Models The verification of results is quite challenging due to missing empirical data of this type and size of drones. Therefore different approaches were followed. We validated the aircraft model by comparing it with flight-test results of a Bo105 and specifications of a Cessna172 (see Figure 34). Nevertheless, these aircraft are classic configurations of passenger-transport size, and it is problematic to scale the validation of their models down.

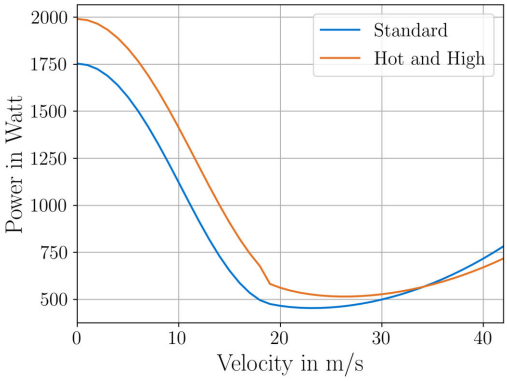

Figure 21: Hot and High

Sensitivity Analysis and Results We performed a Sensitivity Analysis to identify parameters that are critical to the integrity of the results. The Sensitivity Analysis (SA) indicates that the results are very sensitive to the induced power factor, rotor efficiency, aerodynamic drag and mass (see Figure 22). On the one hand, this insight obligates more accurate or conservative modulation of these parameters. On the other hand, this reveals the most promising starting-points of optimization. For the induced power factor, we assumed a more conservative value [18]. The structure mass fraction is also set to the higher value of 0.4 than the often proposed, e.g. 0.35 [1], to get a more conservative estimation of the structure weight. We applied a blade-element-tool provided by Thiele to verify the rotor efficiency and thrust estimation [19]. Chapter 2 already evaluated an accurate model for drag estimation, which was implemented in our model. To verify the mass model's assumptions, we looked for components (motors, rotors, batteries, fuel cells, hydrogen tanks, and aircraft systems) which are available on the market. According to the results of this bottom-up analysis, we adjusted the factors assumed in the top-down mass model.

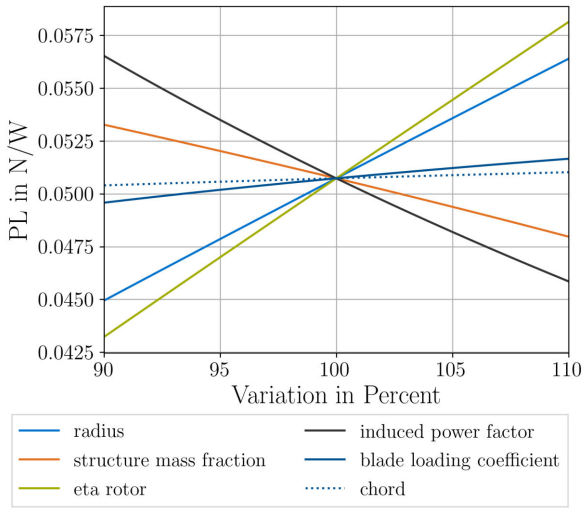

(a) SA Power Loading

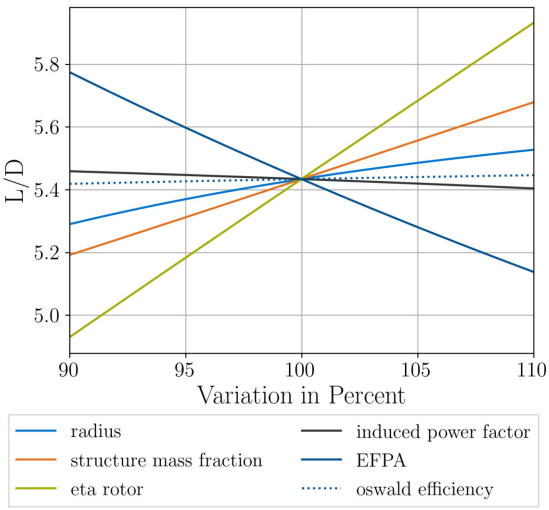

(b) SA Lift over Drag

Figure 22: Sensitivity Analysis

4. Concept of Operations

4.1. Ground Station and Logistic Support

The importance of the ground station should not be underestimated and must be considered in every stage of the design phase. The USAF UAS Flight Plan [61] concludes that immature logistic planning leads to high contractor logistics support expenditures and often causes expensive design changes of the drones.

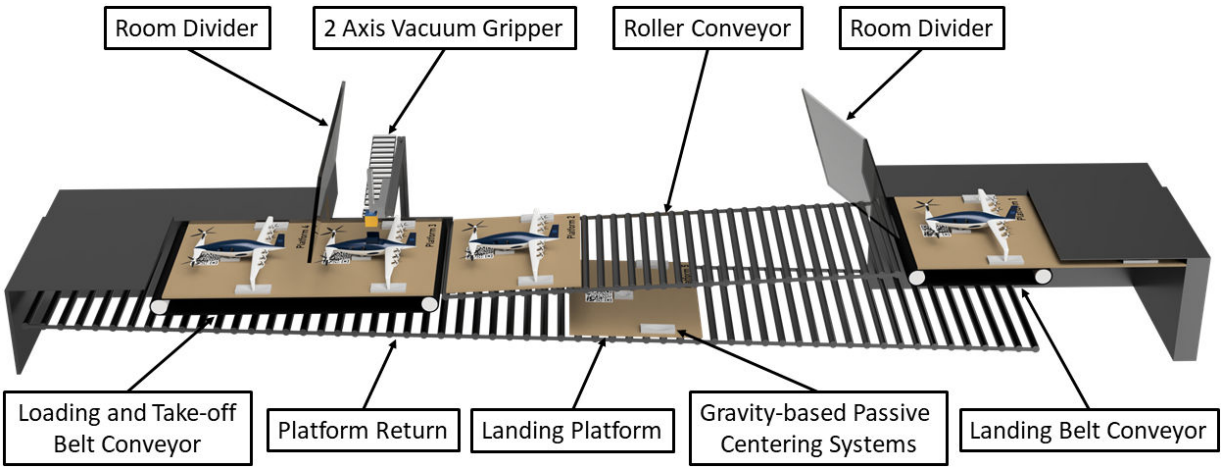

Figure 23: Schematic conveyor belt for package loading (see Appendix Figure 30 for animation video)

Therefore every design decision for the Mercurius Drone was made under consideration of the logistics system at the ground station.

Safety The ground station concept bases on the strict spatial separation of humans from the take-off and landing zone, which significantly reduces the risk of injury to employees. Following the first step of risk reduction "safe by design" [62], it also prevents a collision of simultaneously launching and landing drones. Room dividers separate the areas (Figure 23), to prevent drones from entering the working space.

Setup The entire Mercurius Ground Station is located in a hall with an entry and a departure gate. This setup reduces the risk of drones being caught by winds during hover. The areas' connection occurs through two belt conveyors and a non-driven roller conveyor transporting the drones through the loading, refuelling, or maintenance stations (Figure 23). The approaching drone arrives at the landing plate provided by the first belt conveyor. Afterwards, the landing belt conveyor transfers the drone to the slightly inclined roller conveyor to buffer delivery irregularities. The second belt conveyor carries the Mercurius Drone to the autonomous parcel loading area. Simultaneously, the drone, which has been loaded before is brought to the take-off position. The landing platforms with the gravity-based centering system [63] maintain the exact position of each landing UAV and thus ensure a faultless autonomous dispatch. Ball casters at the ends of the Mercurius drone's legs enable a simple centering process.

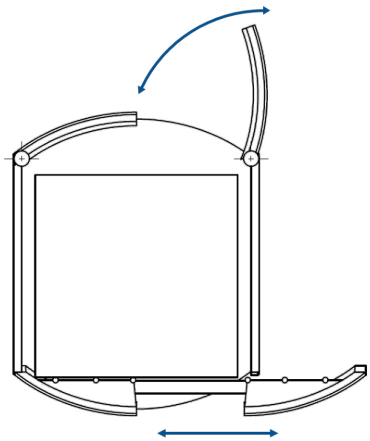

Figure 24: Package Chamber

Package Loading and Drop off Process The Mercurius Drone is loaded from above with a two-axis vacuum gripper that carries the package from its roller conveyor and positions it softly into the drone's cargo chamber (Figure 24). The horizontally opening unloading flaps sustain the cargo inside the drone and remain shut, even if the power supply fails. Foam on the chamber inside prevents the parcel from shifting during transport. At the customers' landing platform, the UAV lands and opens the unloading flaps. The foam in the chamber prevents the package from slipping out too quickly and thus guarantees the integrity of the package. Afterwards, the drone takes off vertically to release the cargo completely and closes the flaps. Customers are not allowed to enter the landing platform as long as the drone performs the drop-off process. The design of the customer landing platform extends the scope of this design challenge and is not further elaborated.

Refuelling and Maintenance The refuelling process is carried out on a separate conveyor (Figure 25). The drone is automatically transported to the secured working area where it is refuelled by an employee. This appears to be the simplest solution for the initial scenario, but refuelling could easily be carried out autonomously by a one-axis tank nozzle with magnetic fittings. Maintenance is also carried out on a separate conveyor lane by an employee from the secured working area (Figure 25). Afterwards, the drone can be easily reintegrated into the delivery system, by shifting it back to the main conveyer belt. This system can easily be expanded with additional runways or double take-off, loading and landing areas. The associated higher parcel throughput and allows the straightforward implementation of automated loading and refuelling. However, the entire infrastructure is demanding to be implemented due to the drone's interface to the conveyor.

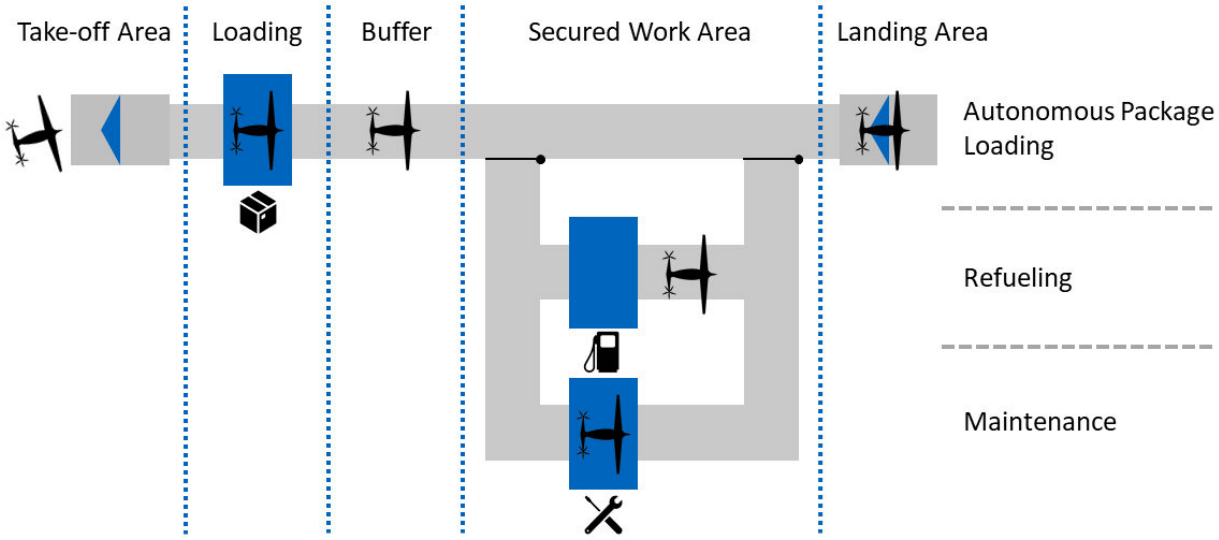

Figure 25: Structure of the Ground Station

4.2. Autonomous Operations

The Mercurius Drone must operate safely within a radius of 15 km around the ground station and has to be suitable for Beyond Visual Line Of Sight Operation (BVLOS). This implies the ability to maintain a stable connection to the Unmanned Aircraft System Traffic Management (UTM) across a wide range, navigate safely, and detect and avoid collisions with other entities within the U-space autonomously. From a regulatory point of view, according to FAA Part 107 BVLOS operations are possible, if the location of the aircraft is known at any time and a Detect and Avoid (DAA) system is in place [64]. In the past, BVLOS operations required a Visual Operator (VO) or ground-based Radar [65]. Within European aerospace, BVLOS operations are limited to a distance of 2 km using VOs for UAS operations regarded as 'specific' [66]. As mentioned in [67], it can be assumed, that BVLOS operations will be possible within a wider range and in urban areas, if the aircraft shows to be compatible with U-space services. Successful examples, such as the delivery route tested by DHL from Norddeich to Juist island in Germany in 2014 [68] or the operations of Zipline Inc. in East Africa and in the U.S. [69], showcase the feasibility of wide-range deliveries in cooperation with aerospace administrations.

Onboard Communications and Identification System In order to communicate with the ground station, the use of voice channels of mobile networks has been found to be advantageous. Positioning data and the identification number are transformed into audio data and transmitted to the ground station. Submitted positioning information is exchanged between the ground station and the UTM. This method provides a stable connection even in rural regions and offers sufficient bandwidth for exchanging information [70]. Other mobile networks like the 3G or 4G band are not suitable, since they are optimized for the sporadic up- and download of larger data packages, resulting in lower reliability [70]. For the integration into the

German UTM, the Droniq Hook On Device (HOD) is the best solution [71]. Combining it with the approved communication via voice channel is a promising option. A severe limit given by the use of voice channels is the low bit rate. Unlike LTE, no exchange of large payload data is possible. However, for near-real-time operations, this is not sensible anyway. Instead, the local processing of complex data on the drone itself is suggested. This method shows to be advantageous regarding privacy concerns, as no footage is submitted to the operator.

Positioning System Similar to Amazon's Visual Simultaneous Localization and Mapping (VSLAM) method [72], the latter is used to overcome connection issues with common GNSSs and guarantees an exact localization of the drone at any time. Therefore, the deployment of pre-trained neural networks reduces the onboard computing effort. The concept includes six cameras with built-in labelling features, such as the FLIR Firefly DL camera [38]. The camera system also contributes to the redundant altimeter system, which includes a barometer, perceives height information from the GNSS and relies on information provided by a Radar directed to the ground.The Radar has a range of more than 150m like the Aerotenna μLanding [73]. For precise satellite positioning, the drone is equipped with a GNSS module like the Here 2 GNSS for Pixhawk 2.1 [74]. It is able to simultaneously receive data from up to three GNSSs including GPS, Galileo, GLONASS and BeiDou and offers multiple redundancies. Additionally, the accelerometer and the gyroscope are used for the Inertial Measurement Unit (IMU), which is reset when landing at the ground station and provides enhanced redundancy. A Kalman filter is used for fusing the sensor data provided by GNSS, VSLAM and IMU [75], to optimize the positioning process.

Detect and Avoid System The DAA system is more important than ever, since the activity in the U-space is expected to increase [67]. Unmanned vehicles, such as logistic drones, have to fulfill certain requirements, in order to avoid incidents with other traffic participants cruising on an altitude of 120 m AGL. Therefore, the DAA system was designed with consideration of the following paradigms [76]:

- stay well-clear of cooperative and uncooperative intruders in regard to defined boundaries like those proposed in [77]
- guarantee at least minimum functionality under rainy and poor lighting conditions, such as fog and low brightness
- act according to air traffic rules
- full compatibility with behavior of other participants and consistent behavior in case two vehicles with the same DAA meet
- interact with the flight control system
- operate autonomously without any human interception
- minimize deviation from the originally planned route
- limit the computational effort in order to save energy and avoid heavy computing units due to the necessity of onboard processing
- react with awareness of the vehicle maneuverability

A comprehensive assessment of several concepts for DAA systems in [78] concludes that "solutions combining a Traffic Collision Avoidance System (TCAS), EO/IR and Radar, seem to be the most feasible ones." In the given case, separation and collision avoidance from cooperative intruders is provided by the UTM in combination with a FLARM device [79], which shows to be suitable for UAVs, i.e. the Mercurius Drone. In German aerospace, FLARM is already implemented within the Droniq HOD [71].
In order to mitigate threats by noncooperative intruders, the system relies primarily on optical computer vision. The implemented Radar system is designed as a backup option. Both systems have distinct drawbacks: Optical solutions are known for suffering the limitation by poor lighting conditions, whereas lightweight Radar systems show a limited range for detecting intruders [80][81]. Nevertheless, computer vision is capable

of working under rainy conditions, since the airflow around the fuselage removes raindrops from the lateral lenses. Additionally, De-raining image processing can be done by using Generative Adversarial Networks (GAN) [82] deployed on the DL cameras. Iris Automation, the first provider of a comparable computer vision DAA system for UAVs, states a detection range of more than 950m for a 360deg field of view system [39]. The FAA calls for a minimum scan radius of two nautical miles for human-driven DAA systems [64], but since the time to react of an autonomous system is negligible, the provided detection range is sufficient.
The feasibility of Radars on drones has been shown by the Fraunhofer FHR [80]. The ability to detect small unmanned aerial vehicles has been proven by the Fraunhofer HHI [83]. Commercially available solutions are, for example, provided by Aerotenna [81]. The detection range of these Radar systems is limited to 150 m, wherefore they can only serve as last-moment collision avoidance if the optical computer vision system fails. In case the optical system is disturbed by dense fog, smoke or malfunction, the aircraft reduces its speed, so that the DAA function can be safely provided by Radar. The aircraft is equipped with one Radar device in flight direction and two laterally located ones like it is shown by Aerotenna [73].
In order to evaluate the well-clear status of aircraft and to provide a range of possible flightpaths in case a loss of separation might appear, the open-source NASA software Detect and Avoid Alerting Logic for Unmanned Systems (DAIDALUS) [84] is used. Furthermore, the decision about the selected flight path will be made by software built upon Independent Configurable Architecture for Reliable Operations of Unmanned Systems (ICAROUS) [85], which has been developed for NASA's UTM program and is meant to rely on the well-clear information provided by DAIDALUS. Further refinement of the final flight path selection in compliance with the mentioned paradigms can be realized by using a learning-based mechanism like shown in [86].

4.3. Mission Profile and Number of Drones

Launching a drone with a package every two minutes is one specified essential requirement [9]. On the one hand, multiple drones can be used. On the other, the mission duration can be shortened. To reduce the number of required drones to a minimum and to save costs, a drastic reduction of the mission time is inevitable. Therefore, we use the advantages of the hybrid configuration and deliver three parcels with one tank filling. Compared to one package per tank, only a third of stops for refuelling is needed and saves time. Furthermore, the charging process of a battery concept is significantly higher, which requires additional drone capacity. Nevertheless the high travel speed of 42 m/s also helps to save even more time.
Figure 26 illustrates the mission profile of one tank filling. The time assumptions of the individual operations enable three parcels deliveries within an 80 minutes time window:

- The ground processing of the drone with transportation and parcel loading takes three minutes.
- The total flight time for delivering a package and returning to the base takes a maximum of 20 minutes for a distance of 30 km.
- For the parcel drop of at the customer, one minute is calculated.
- Eight minutes are considered for refuelling and as a buffer.

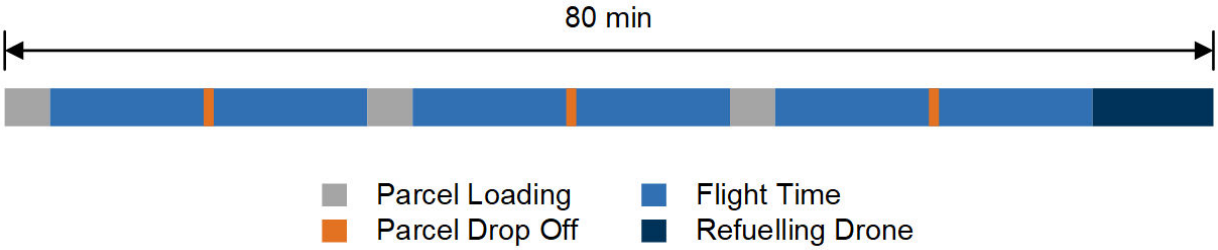

Figure 26: Mission profile with one tank filling

The calculations of the idealized mission profile are quite conservative, because the mission cycle is a very dynamic process and hard to plan precisely. Starting with the distance to the customer that can be shorter

and will not always be the full 15 km or further weather conditions are changeable and have a significant impact on flight time. Also, the three minutes of ground processing time will mostly be undercut. Since there are almost always a few drones as a buffer in the ground station's handling line, the individual work steps can be carried out simultaneously on different drones. Therefore, the three-minute window refers to the maximum time interval between the arrival of a drone, the parcel loading, and the departure of a drone, which may be another one that has already been on the ground station before. Nevertheless, the assumptions mentioned above serves as a reasonably good estimation. It is therefore certain what number of drones will be needed in case of bad conditions. With a buffer of 25 % additional vehicles, the two-minute delivery interval is observed with 17 drones. For a battery concept at least 39 aircrafts are necessary .

5. Safety Analysis

The Mercurius Drone's design with its unique propulsion system and DEP is a very failure tolerant configuration. Additionally, it features many redundancies regarding the communication system and the DAA system. To verify this high level of safety, a fault tree analysis (Figure 27) quantifies the failure probability λ per flight hour of certain functions[87]. In this chapter, the procedure is explained with the function "provide lift". The failure tree is structured from aircraft level to system level with assumed failure probabilities of λ per flight hour for each system. These values are used to calculate the expected failure probabilities on higher levels using 'AND' and 'OR' relations according to the bottom-up principle. In this example, the 'Loss of Lift' case is considered. For DC Brushless electric motors, we considered a lambda of $\lambda \leq 1.3 * 10^{-5}$ for one motor [88]. Regarding the front wings, a loss of one motor already leads to a complete loss of lift in a conservative approach. Besides, we assumed a significant loss of rear-wing lift in case two out of three engines of either the starboard or the port side are lost. The failure behavior is modeled using a Markov Model for a loss of two components out of three. All four systems are linked by an 'OR' gate because already one of the four cases leads to a total loss of lift.
Should the energy supply fail, a loss of lift is not triggered directly: During the cruise, enough power margins by the remaining energy source ensuring a continued flight or at least an emergency landing. For the hovering aircraft, we assess the margins acceptable to ensure a soft landing. To be more precise, an 'AND' gate may be used leading to a high degree of reliability in the energy supply system, although relevant Mean Time Between Failures (MTBF) has been selected conservatively [89][90].
According to the Fault Tree, the failure condition 'Loss of lift' is triggered by either a 'Critical Loss of motors' or a 'Loss of power' and is hence subject to a failure rate of λ of $2.8 * 10^{-5}$. To limit the failure effect of a 'Loss of lift' for people and property, we introduce a total failure system with an esteemed probability of failure as a backup safety measure. It should be mentioned again that the parachute requires a minimum altitude of 9 m. We may disregard this fact for the analysis since an altitude of under 9 m only applies to takeoff and landing where no humans are in the hazardous area.

Conclusion There are many other systems to be considered, such as the software or the flap systems. The example fault tree shows that by 'OR' coupling, the 'Catastrophic loss of lift', i.e., an unbraked and thus dangerous crash for humans, reaches a probability of $\leq 2.9 * 10^{-9}$ per flight hour. This translates into a 'Catastrophic loss of lift' every MTBF = 344827586 flight hours. Calculated to 8h, a fleet of 17 drones and 300 operating days, the first drone crashes with a faultless opened parachute on average after 0.875 years, and a catastrophic crash with a malfunctioned total failure system occurs after a mean time of 8452 years. This calculation only refers to a crash due to the malfunctions mentioned here (Figure 27).
However, a fault tree analysis will not be necessary for the certification, but it leads to an intuitive estimation of the Mercurious Drone's safety.

Hydrogen Fuel Cell Safety The drone's propulsion system cannot be chosen without the full guarantee of safety for humans and the environment. Since hydrogen has a very low density and is 13 times lighter than air under normal conditions, it must be brought to a high pressure of 350 bar for the application in the Mercurious Drone. A hydrogen-air mixture with a hydrogen content between 4% and 77% is combustible with a

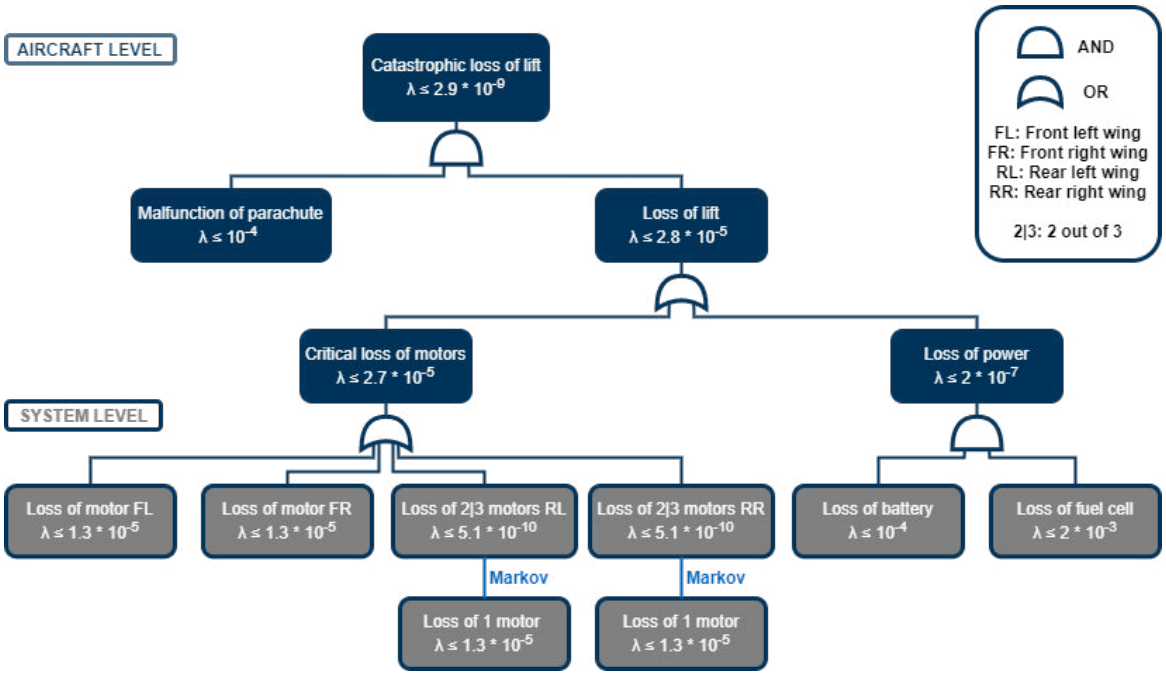

Figure 27: Exemplary fault tree for the probability of failure λ per flight hour

minimal energy supply, hence the concern about lack of safety has often spread among the population.[36]

To counteract this, the production of hydrogen tanks is carried out under strictly standardized safety requirements [36]. Hydrogen tanks of this type are safe against impact, fire and overpressure [91]. Toyota, for example, fired bullets at its own hydrogen tanks. Only from caliber .50 on, the tank leaked under repeated shooting on the same spot, whereby the escaped hydrogen did not endanger the environment [92]. In case of fire or overpressure, the hydrogen can be discharged in a controlled manner using a PRD. This is particularly useful in aviation, as the hydrogen volatilises far away from ignition sources, which are usually located near the ground [36, 37].

These properties make the hydrogen-powered fuel cell a safer propulsion system than the lithium ion battery, which suffers from a high risk of burning at excessive temperatures due to its intrinsically flammable electrolytes [93]. In [94] different energy sources were compared, with the authors giving the hydrogen fuel cell a safety rating of 10/10 and the lithium ion battery a rating of 6/10. These advantages in operational safety were an important part of the decision for the hybrid fuel cell configuration as the propulsion system for the Mercurius drone.

6. Business Scenario

Our vision of a comprehensive Mercurius delivery service can only be enforced if it is economically profitable. The market analysis, which we have presented in Section 1.1, defines the rough framework conditions. In the process of a first market launch, it is essential to focus on the 25% of consumers that are willing to pay more for on-demand instant delivery service in urban and rural areas. Operating Mercurius in this yet undeveloped and challenging business area promises the most significant economic opportunities for the future. The expansion of the target group will be set in a later step. Bringing the vision of delivery times shorter than 30 minutes between ordering and receiving the product to life requires an economically viable business scenario, which we describe in the following.

6.1. Calculation of Costs

The detailed investigation of the various costs that consist of capital expenditures for the aircraft, the ground station and operational expenditures allows us to make a more realistic statement about the package's delivery price than other competitors. The choice of the hybrid configuration also turns out to be the result of this analysis. The Mercusius Drone offers refuling times of five minutes insted of over an our in the battery powered case. This efficient aircraft utilization due to drastically reduced ground time is the most significant cost saver.
The detailed cost analysis is exemplary calculated on the basis of one operating ground station and is divided into two scenarios. At a first more conservative approach at initial use, costs are calculated using values and parameters that are currently technically feasible. Subsequently, in a more optimistic long-term scenario, these values and strategies are adjusted, which can be achieved with higher production levels and more experience. In order to ensure comparability, all costs are stated in US dollar prices.

Costs of Aircraft The costs for the aircraft are divided into the material costs and manufacturing costs. The costs of the powertrain requires special consideration. Prices of hydrogen fuel stacks have fallen by 60% over the past decade, and are expected to further decrease [95]. The U.S. Department of Energy (DOE) estimates the 2019 costs of fuel cell systems at low production numbers at 180 $/kW with additional costs of 21 $/kWh for a tank system [95]. With these calculations we would get $174 for the fuel cell configuration and $220 for the battery version, whereby the price for a lithium ion battery was calculated at high production numbers in 2020 [96]. In the conservative scenario we nevertheless assume $300 for both propulsion systems for the sake of comparability. Table 8 shows a list of the individual cost components. The high costs for the Aircraft Systems are particularly noticeable. Common structural materials such as depron and glass fibre [97] are cheap, but the manufacturing costs must also include the costs of shaping and fabricating the structure with different machines.

Parameter	Conservative
Fuell Cell System	$300
Aircraft Systems	$5270
Structure	$300
Engines for Propellers	$320
Servos for Control	$75
Security System	$300
Manufacturing Costs	$3999
Total Costs	$10664

Table 8: Costs of Aircraft

In addition to the material costs of the aircraft, we assume initially high manufacturing costs of 60% of the material costs and thus arrive at a realistic total cost of $10664. This way, we end up with a similar cost prediction as [101]. The costs calculated in other papers (e.g. [102]) are often much cheaper, while expensive autonomous flight and safety systems are mostly neglected. With increasing production figures and decreasing material costs, we assume a reduction in costs of 40% in the optimistic scenario, whereby this assumption is more conservative than others that calculate long-term costs with 16% of the initial value [14].

Parameter	Conservative
Logistics area sqm	$300
Maintenance area sqm	$50
Maintenance per sqm	$6.05
Land value per sqm	$121
Machinery	$15000
Electrolyzer	$15000
Compressor	$2500
Total Overhead Costs	$689400

Table 9: Costs of Ground Station including reference values from [98],[99],[100]

Installation Costs The ground station consists of an parcel warehouse and an autonomous handling area where the drones are loaded and refuelled. For the case of 17 operated drones we calculate with a serviceable area of 350 m^2, which is composed of logistics area and repair area (see Table 9). The development of unused roof areas, cooperation with big parcel shipping companies like DHL or the shift to rural areas would have a signifcant cost advantage.

The need for more infrastructure by the hybrid concept has a certain disadvantage in comparison to battery concept. The hydrogen demand on the ground is covered by on site electrolysis. We assumed a state of

the art efficiency of 85% [100]. In addition, a compressor is nesscessary. This requires an additional energy input of 2.9 kWh/kg-H2, which must be included in the calculation [103]. The charging infrastructure of the battery-powered concept were neglected in our calculations.

Operating Costs Aircraft The use of hydrogen has the advantage of providing the energy carrier cost-effectively with cheap off-peak electricity prices during night. In this way, the electricity costs can be reduced compared to the battery configuration. For the latter, we assume an average international electricity price of 18 ct/kWh in both scenarios and a 30% saving by using cheaper tariffs for the hydrogen configuration [104]. The use of old hybrid batteries of the parcel drone in the ground station in a second live approach can further reduce the costs. With dynamic pricing tariffs, cheaper electricity can be temporarily stored and thus supply the ground station with energy at expensive prices. We assume a moderate depreciation period of four years for our aircraft, with the drones being resold at 10% of the purchase price at the end of the period [101]. For a mainenance cost estimation, we assume an annual 5% of the aircraft cost for Propeller replacement and smaller repairs like mentioned in [101].
There are various providers of drones liability insurances. Nevertheless, our use case is not covered because of its novelty. As estimation [105] assumes annual costs of about $500 to $2200 per aircraft, but it can be anticipated that prices will continue to decrease in the future [106]. Using the airspace is considered with costs either, which should not be neglected. According to [102] $2.26 per hour per aircraft is assumed. We are aware that this value can still vary considerably.

Operating Costs Groundstation Since our conservative scenario assumes aircraft refueling by hand, human labor is unavoidable. The conservative assumption is made by two full-time employees, causing employer costs of $30.25, which is the average of the EU [107]. In the optimistic case, these labor costs are reduced to one employee working 40% of the operating time, since the autonomous station does not require as much supervision. However, we charge the station maintenance at an annual cost of $6.05 per sqm [98].

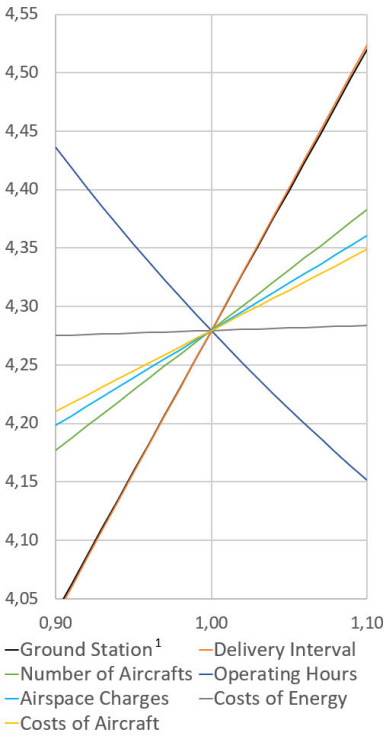

Figure 28: Costs per delivery sensitivity analysis

Summary of Costs A more precise understanding of costs' composition is achieved by a sensitivity analysis of the conservative scenario. Figure 28 shows the most signifcant parameters. In addition to the apparent cost drivers, such as the number of drones, it is traceable where adjustments appear particularly profitable and where not. The shortening of delivery intervals leads to an enormous cost reduction, despite the additional drones. The optimum will be achieved by the shortest possible delivery interval without major modifications of the ground station. Labour costs also appear to have an strong impact on the delivery price. Implementing autonomous ground station processes on a large scale is thus critical to secure competitiveness in the long run. Unfortunately the high acquisition costs of the ground station are pretty set. Future cost reductions for such systems and the integration into existing logistics systems are a major opportunity to push the delivery price further downwards. Another variable with significant influence is the operating time of the service. On the one hand the number of operating days per year and on the other hand the operating hours per day. Due to extreme weather events and countries with tight labor laws such as Germany, the operational days of about 300 per year will be subject to minor changes. However, a change from pessimistic 8 to optimistic 12 operating hours seems feasible. Changing airspace charges also substantially impact the final price tag but unfortunately, cannot be influenced by us. Figure 29 summarises all the assumptions of the conservative and optimistic scenario and quantifies the delivery costs per package of $4.30, respectively $1.08. Comparative calculation shows that the hybrid configuration is about 30% cheaper than a battery configuration due to better utilization.

[1] Including Costs of Employees

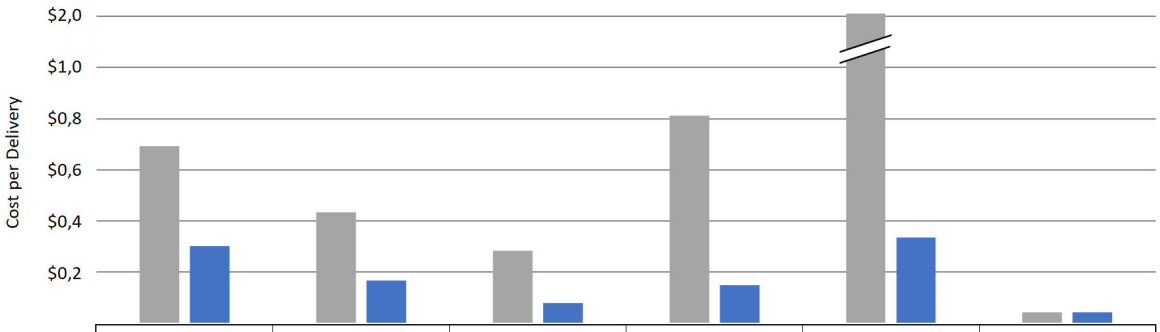

	Aircraft incl. Maintenance	Ground Station incl. Maintenance	Insurance	Airspace Charges	Ground Personnel	Fuel Costs
Pessimistic	0,69	0,43	0,28	0,81	2,02	0,04
Optimistic	0,30	0,17	0,08	0,15	0,34	0,04

Figure 29: Summary of Costs per Delivery

6.2. Regulatory Aspects

To meet the latest certification requirements, the EASA requirements for UAV operations in the "Specific" or "Certified" Category [108] including the JARUS SORA path [109], and FAA Part 107 [64] as well as Part 135 [110] must be considered. In the USA, UPS Flight Forward, Inc. was the first company to be certified to FAA Part 135 [111], but its operation is limited to remote-controlled BVLOS operation. For certification in the European area, the requirements of the "Specific" or "Certified" category of the EASA must be observed. According to our analysis of the JARUS SORA path, a certification according to "Specific" for remote control would already feature an overall Specific Assurance and Integrity Level (SAIL) 4 [109]. Our assessment shows to be realistic as comparable concepts like the Avy wing drone are developed in compliance with EASA BVLOS SORA SAIL 4-6 [112]. The certification of any type of operation seems to be a decisive advantage of SORA and thus offers the most possibilities for certification of our UAV operation. Current certification regulations refer to Remote Pilots BVLOS operations and do not explicitly specify fully autonomous vehicles, but the authorities are working on extensions and new regulations [113].

6.3. Competitive Ability

The Mercurius concept offers fast, quiet, and cost-competitive delivery at the highest safety level. Its innovative and highly integrated ground station promises an outstanding potential for automatization of delivery services. Therefore it is flexible in applying and economically attractive. A comparison with other drone concepts in Table 10 underlines these theses.

Drone	Max Payload (kg)	Max Range (km)	v_{cruise} (km/h)	Autonomy Level
Avy [112]	2.5	130[1]	130	fully
Ehang Falcon B [114]	5	19	80	low
EmQopter [115]	2	3	70	fully
Volans-i C10 - Gen 2 [116]	4.5	80.5[1]	96.6	partly
Wingcopter [117]	6	120[1]	100	high [118]
Mercurius	6	174[1]	151.2	fully

Table 10: Comparison with Competitors

Especially the calculations in the optimistic scenario show the enormous potential of the delivery service in the future, which is clearly superior to conventional delivery services within the price range of $2 to $8 [119]. At the same time, the analysis gives a more realistic assumption, since parameters like the costs per aircraft

[1] Range without Payload

and the ground station are often assumed too low or neglected completely in papers such as [120] and [102]. Besides existing drone delivery services, the biggest competition operates from the ground. However, the usual delivery service strategy with vehicles or bikes reaches its limits and cannot adequately cover the growing demand for same-day and instant delivery. Especially the request of 73% of the customers for more flexibility in precise delivery time slots [121] is beyond reach. This is where the Mercurius delivery concept's advantages come into their own. No significant preparations and route planning are necessary, and the buffer of drones in the ground station allows a quick response to new requests, where conventional delivery services would fail. Besides this, precise time slots have the advantage that the customer is most likely to be on-site and can better schedule and adjust his day regardless of the parcel delivery. Therefore, missing customers and setting up alternative pick up points in case of unsuccessful delivery are things of the past.

According to [122], there is a significant increase in the delivery price if the time window is tiny. For a one hour time window in densely populated areas, one delivery costs approximately $6. The price continues to rise in more sparsely populated areas. Ideally, prices range between $2 and $3 per package, including bike delivery, and even these can be met by Mercurius [122].

Consequently, the service must be very reliable, which is a further advantage over conventional delivery methods by Mercurius. It cannot be stuck in traffic jams like vehicles or face unforeseen obstacles as even bicycle couriers can. In addition, the modular ground station offers excellent flexibility and can be easily varied in size to suit the respective application. Consequently, the delivery interval can be shortened quite easily. Last but not least, our concept has benefits in terms of costs.

7. Conclusion

With the Mercurius Concept presented, many hurdles that previously stood in the way of a scalable use of parcel drones are overcome.

- The aerodynamic design combines interfering requirements of high power loading and high aerodynamic efficiency
- With innovations like downwarded winglets or top-wing props a maximum L/D ratio of over 6 is achieved despite low Reynolds numbers, while other concepts (e.g. Amazon) end up with estimated values of 3 [1]
- The use of a hybrid fuel cell opens the path to high ranges and mission radiuses as well as to efficient utilization of the aircraft
- Fully automated flight navigation enables autonomous flight operations and integration into the UTM
- The redundant hybrid propulsion system, high safety of the fuel cell and the redundant engines help the Mercurius Drone to achieve maximum flight safety
- In an unlikely event of a total failure, a parachute airbag configuration prevents damage to the aircraft and the environment
- Complex autonomous battery exchange units or a high number of aircrafts are not necessary with the hydrogen configuration
- The presented ground station concept offers the possibility to variably adjust and increase the required handling interval of 120s
- These measures bring the price per package down to $1.08, covering costs up to the complete ground station. This makes the Mercurius Drone 30% more economical than a comparable battery concept

The question of scalability and feasibility on a large scale naturally remains. Several start-ups are concerned with autonomous delivery service operating with small vehicles on the ground. This approach may even be superior to drones in urban areas. However, specific applications like instant delivery, hard to reach places or not high densely populated areas where the higher range of Mercurius comes into weight are the sweet spots of the air delivery. If the hurdles of further testing, certification and the choice of appropriate use cases are overcome, a concept like the Mercurius Drone is ready to revolutionize the new instant delivery market.

A. Appendix

Ground Station Video

Figure 30: Ground Station Video: Scan barcode or visit link (https://a360.co/3iVlNqd)

Further Performance Data

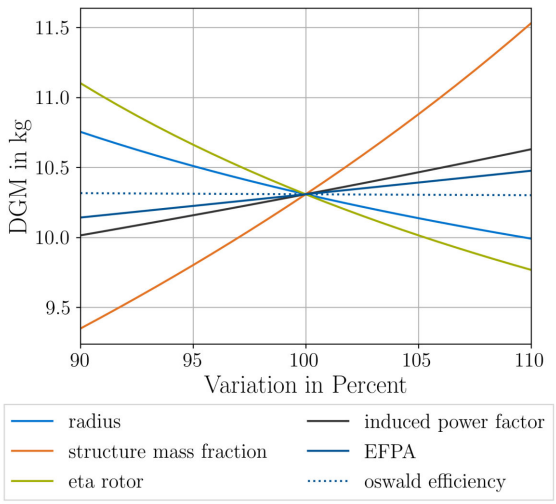

(a) SA Design Gross Mass

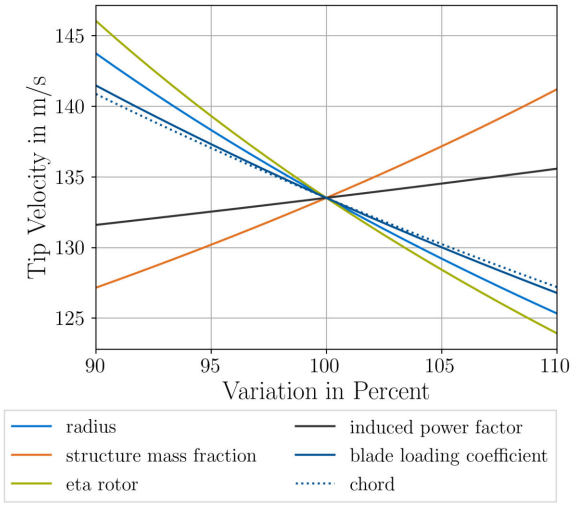

(b) SA Blade Tip Velocity

Figure 31: Sensitivity Analysis

Property	Value
Wing Area	0.048 m^2
Taper	0.66
Profile	NACA23012

Table 11: Wing Front

Property	Value
Wing Area	0.2 m^2
Taper	0.66
Profile	NACA23012

Table 12: Wing Rear

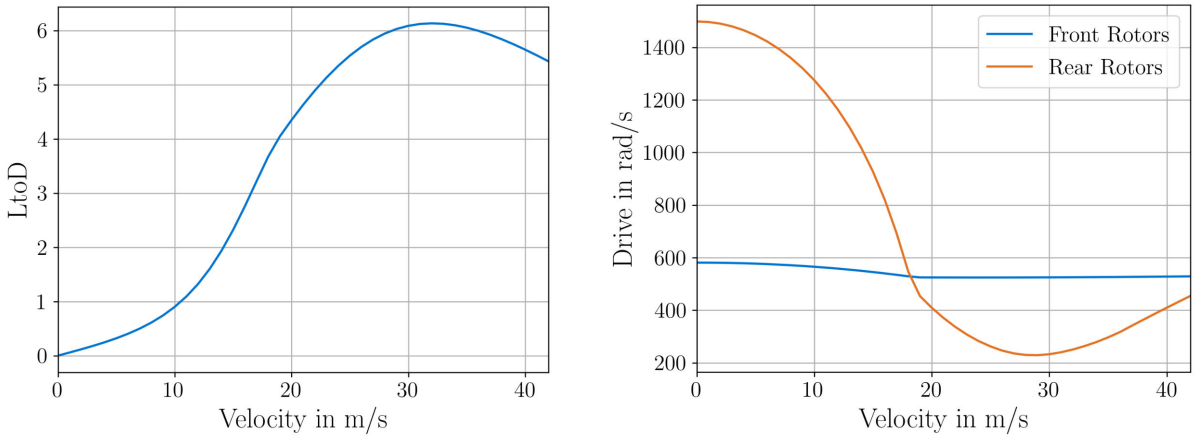

(a) Lift over Drag Ratio

(b) Drive across Flightstates

Figure 32: L/D ratio and drive of rotors

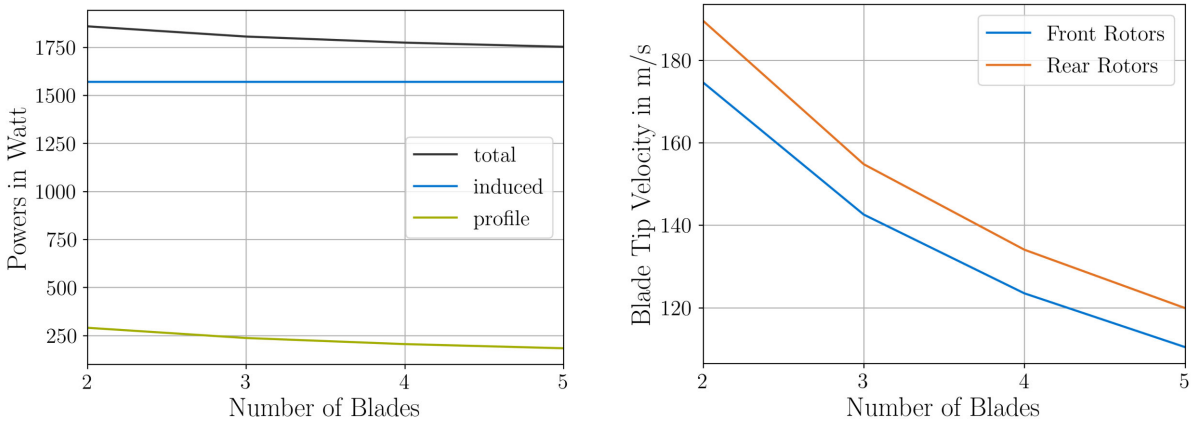

(a) Power

(b) Tip Velocity

Figure 33: Power and tip velocities over varying numbers of propeller blades

Property	Value
Number of front Rotors	2
Radius	0.19 cm
Number of Blades	5
Blade Loading	0.12
Drag Coefficient (cd_0)	0.011
Induced Power Factor	1.2
Efficiency	0.85

Table 13: Rotors Front

Property	Value
Number of rear Rotors	6
Radius	0.06 cm
Number of Blades	5
Blade Loading	0.12
Drag Coefficient (cd_0)	0.011
Induced Power Factor	1.2
Efficiency	0.85

Table 14: Rotors Rear

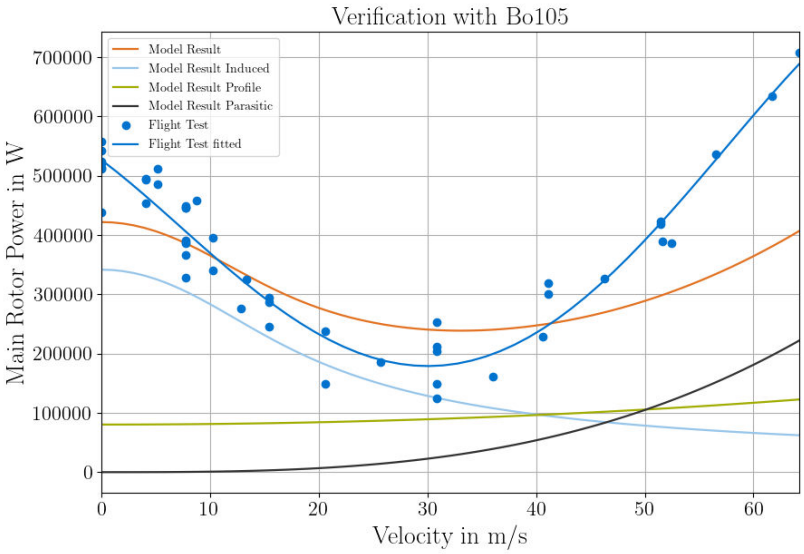

Figure 34: Verification with Bo105

This plot presents the results of the Bo105 implemented in the used aircraft model and in real flight. The model of a Cessna172 also matches the power requirements of 134 kW at 233 km/h and mean sea level.

Aircraft Systems Costs

Component	Weight (g)	Cost ($)	n
DL Cameras + lenses [38]	30	275	6
GNSS unit [74]	49	115	1
Flight Controller [123]	250	350	1
Radar [81]	22	700	4
Ultrasonic sensor [41]	5	3	1
Computing/Communications	250	300	1
Microphone	16	6.45	1
Control System for ANC	36	38	1
Speaker	68	7.6	1
Total	1062	5270	

Table 15: Sensors and computing units

Business Scenario

general parameters	value
electricity price ($/kWh)	0,12
energy density H2 (kWh/kg)	33,33
operational days per year	300
max. operating time per day (h)	12
delivery interval (s)	100
delivered packages per hour	36

aircraft parameters	value
number of aircraft active	16,31
total number of aircraft	20,39
costs of aircraft	6398,4
depreciation period aircraft (years)	4

ground station parameters	value
costs ground station	502240
depreciation period ground station (years)	25
costs electrolyser per kW ($/kW)	1000
depreciation period electrolyser (years)	25
costs compressor	1750
depreciation period compressor (years)	25
electrolyser efficiency	0,8

aircraft operating costs parameters	value
insurance costs per aircraft per year	500
charges for one hour use of airspace per airc	0,5
aircraft maintenance	0,05
required energy tank (kWh)	0,8
time until next refueling (s)	4894
efficiency FC (already included in energy)	1

operating costs ground station parameters	value
number of staff	0,4
hourly wage of staff	30,25
maintenance ground station	0,02
energy consumption compressor (kWh/kg)	2,9

result aircraft	value
Depreciation costs of aircraft per h ($)	8,15

result ground station	value
depreciation costs ground station per h ($)	5,02
depreciation costs electrolyser per h ($)	0,13
depreciation costs compressor per h ($)	0,02

result aircraft operating costs	value
insurance costs per hour	2,83
airspace charges per hour	5,38
maintenance aircraft per hour	2,72
number of refuelling per hour Hydrogen	12,00
required amount of H2 per aircraft (kg)	0,024
required amount of H2 per hour (kg/h)	0,288
required amount of H2 per day (kg/d)	3,46
required power electrolyser (kW)	12,00
electrolyser costs ($)	12000
electricity cost per compressed kg(H2) ($)	5,35
cost of tank filling ($)	0,13

result operating costs ground station	value
costs personnel per hour	12,1
maintenance ground station per hour	0,88

total costs	value
costs per hour ($)	38,78
costs per package ($)	**1,08**

general parameters	value
electricity price ($/kWh)	0,18
operational days per year	300
max. operating time per day (h)	12
delivery interval (s)	100
delivered packages per hour	36

aircraft parameters	value
number of aircraft active	36,91
total number of aircraft	46,14
costs of aircraft	6398,4
depreciation period aircraft (years)	4

ground station parameters	value
costs ground station	502240
depreciation period ground station (years)	25

aircraft operating costs parameters	value
insurance costs per aircraft per year	500
charges for one hour use of airspace per airc	0,5
aircraft maintenance	0,05
required energy battery (kWh)	0,55
time until recharching (s)	7383

operating costs ground station parameters	value
number of staff	0,4
hourly wage of staff	30,25
maintenance ground station	0,02

result aircraft	value
Depreciation costs of aircraft per h ($)	18,45

result ground station	value
depreciation costs ground station per h ($)	5,02

result aircraft operating costs	value
insurance costs per hour	6,41
airspace charges per hour	5,38
maintenance aircraft per hour	3,26
number of refuelling per hour	18,00
cost of tank filling ($)	0,099

result operating costs ground station	value
costs personnel per hour	12,1
maintenance ground station per hour	0,88

total costs	value
costs per hour ($)	53,29
costs per package ($)	**1,48**

Figure 35: Economic Study Optimistic Scenario: Fuel Cell (left) Battery (right)

References

[1] Jia Xu. *Design perspectives on delivery drones*. RAND, 2017.

[2] Pitney Bowes. *Pitney Bowes Parcel Shipping Index*. 2019. URL: https://www.pitneybowes.com/us/shipping-index.html (visited on 05/28/2020).

[3] Economist. *The hidden cost of congestion*. 2018. URL: https://www.economist.com/graphic-detail/2018/02/28/the-hidden-cost-of-congestion (visited on 05/27/2020).

[4] Joshuah K Stolaroff et al. "Energy use and life cycle greenhouse gas emissions of drones for commercial package delivery". In: *Nature communications* 9.1 (2018), pp. 1–13.

[5] Marsh. *Drones – A View into the Future for the Logistics Sector?* 2015. URL: https://www.marsh.com/uk/insights/research/drones-view-into-the-future-for-the-logistics-sector.html (visited on 06/03/2020).

[6] SESAR Joint Undertaking. "European drones outlook study. Unlocking the value for Europe". In: *SESAR, Brussels* (2016).

[7] Martin Joerss et al. "Parcel delivery: The future of last mile". In: *McKinsey & Company* (2016).

[8] Davies and Robson. *LAST MILE DELIVERY: IMPROVING FIRST-TIME SUCCESS*. 2020. URL: https://www.daviesrobson.co.uk/news/delivering-on-last-mile-expectations/ (visited on 06/28/2020).

[9] Challenge Criteria. *Joint NASA/DLR Design Challenge 2020*. URL: https://www.dlr.de/content/de/artikel/nachwuchs/nasa-dlr-design-challenge.html (visited on 06/15/2020).

[10] The Verge. *Delivery drones are coming: Jeff Bezos promises half-hour shipping with Amazon Prime Air*. 2013. URL: https://www.theverge.com/2013/12/1/5164340/delivery-drones-are-coming-jeff-bezos-previews-half-hour-shipping (visited on 05/27/2020).

[11] Marc P Narkus-Kramer. "Future demand and benefits for small unmanned aerial systems (UAS) package delivery". In: *17th AIAA Aviation Technology, Integration, and Operations Conference*. 2017, p. 4103.

[12] Statista. *Prognostiziertes weltweites Marktvolumen der autonomen Last Mile-Lieferung in den Jahren 2019 und 2030*. 2020. URL: https://de.statista.com/statistik/daten/studie/1125733/umfrage/marktvolumen-der-autonomen-last-mile-lieferung/ (visited on 07/01/2020).

[13] Dario Floreano and Robert J Wood. "Science, technology and the future of small autonomous drones". In: *Nature* 521.7553 (2015), pp. 460–466.

[14] UBER Elevate. "Fast-forwarding to a future of on-demand urban air transportation". In: *Uber. com* (2016).

[15] *Systems Engineering for Aerospace*. Elsevier, 2019. ISBN: 9780128164587. DOI: 10.1016/C2018-0-00485-5.

[16] Egbert Torenbeek. *Advanced aircraft design: Conceptual design, analysis and optimization of subsonic civil airplanes*. Aerospace series (Chichester, England). Chichester: Wiley, 2013. ISBN: 9781118568118. URL: http://lib.myilibrary.com?id=487322.

[17] Ajoy Kumar Kundu, Mark A. Price, and David Riordan. *Conceptual Aircraft Design : An Industrial Approach*. Newark, UNITED KINGDOM: John Wiley & Sons, Incorporated, 2019. ISBN: 9781119500261. URL: http://ebookcentral.proquest.com/lib/munchentech/detail.action?docID=5625431.

[18] J. Gordon Leishman. *Principles of helicopter aerodynamics*. 2. ed. Vol. 18. Cambridge aerospace series. New York, NY: Cambridge Univ. Press, 2006. ISBN: 978-0-521-85860-1. URL: http://www.loc.gov/catdir/enhancements/fy0633/2005025467-d.html.

[19] Moritz Thiele. "Erweiterung und Validierung eines Rotortools mit Vorbereitung einer Konfigurationsstudie". Masterarbeit. München: Technische Universität München, 7.09.2016.

[20] Tobias Wirth and Manfred Hajek. “Probabilistic Methodology for Multi-Fidelity Model-Based Robust Preliminary Design of Rotorcraft”. In: *AHS International 73rd Annual Forum & Technology Display, Fort Worth, Texas* (2017).

[21] HB Wang, Z Zhou, XP Xu, and XP Zhu. “Influence analysis of propeller location parameters on wings using a panel/viscous vortex particle hybrid method”. In: *The Aeronautical Journal* 122.1247 (2018), pp. 21–41.

[22] Pierluigi Della Vecchia, Daniele Malgieri, Fabrizio Nicolosi, and Agostino De Marco. “Numerical analysis of propeller effects on wing aerodynamic: tip mounted and distributed propulsion”. In: *Transportation research procedia* 29 (2018), pp. 106–115.

[23] Shahriar Khosravi and David W Zingg. “Aerostructural perspective on winglets”. In: *Journal of Aircraft* 54.3 (2017), pp. 1121–1138.

[24] Werner Nachtigall and Alfred Wisser. *Bionik in Beispielen: 250 illustrierte Ansätze*. Berlin: Springer Spektrum, 2013. ISBN: 978-3-642-34766-5. DOI: 10.1007/978-3-642-34767-2.

[25] Wanyi Ng and Anubhav Datta. “Hydrogen Fuel Cells and Batteries for Electric-Vertical Takeoff and Landing Aircraft”. In: *Journal of Aircraft* 56.5 (2019), pp. 1765–1782.

[26] Zhan Lin, Tiefeng Liu, Xinping Ai, and Chengdu Liang. “Aligning academia and industry for unified battery performance metrics”. In: *Nature communications* 9.1 (2018), pp. 1–5.

[27] Jin-Yi Li et al. “Research progress regarding Si-based anode materials towards practical application in high energy density Li-ion batteries”. In: *Materials Chemistry Frontiers* 1.9 (2017), pp. 1691–1708.

[28] Yasuhiro Nonobe. “Development of the fuel cell vehicle mirai”. In: *IEEJ Transactions on Electrical and Electronic Engineering* 12.1 (2017), pp. 5–9.

[29] Fandi Ning et al. “Flexible and lightweight fuel cell with high specific power density”. In: *ACS nano* 11.6 (2017), pp. 5982–5991.

[30] Bruno G Pollet, Shyam S Kocha, and Iain Staffell. “Current status of automotive fuel cells for sustainable transport”. In: *Current Opinion in Electrochemistry* (2019).

[31] Christian Mohrdieck, Massimo Venturi, and Katrin Breitrück. “Mobile Anwendungen”. In: *Wasserstoff und Brennstoffzelle*. Springer, 2017, pp. 59–113.

[32] Ninni Sofie Brun. “Preliminary design of a fuel cell-battery hybrid propulsion system for a small VTOL UAV”. MA thesis. University of Stavanger, Norway, 2018.

[33] Jih-Sheng Lai and Michael W Ellis. “Fuel cell power systems and applications”. In: *Proceedings of the IEEE* 105.11 (2017), pp. 2166–2190.

[34] Nammin Lee et al. “Parametric study of passive air-cooled polymer electrolyte membrane fuel cell stacks”. In: *International Journal of Heat and Mass Transfer* 156 (2020), p. 119886.

[35] Koji Yamazaki and Yohsuke Tamura. “Study of a post-fire verification method for the activation status of hydrogen cylinder pressure relief devices”. In: *International Journal of Hydrogen Energy* 42.11 (2017), pp. 7716–7720.

[36] Ulrich Schmidtchen and Reinhold Wurster. “Sicherheit in der Anwendung von Wasserstoff”. In: *Wasserstoff und Brennstoffzelle*. Springer, 2014, pp. 43–58.

[37] Zhiyong Li and Yiying Luo. “Comparisons of hazard distances and accident durations between hydrogen vehicles and CNG vehicles”. In: *International Journal of Hydrogen Energy* 44.17 (2019), pp. 8954–8959.

[38] *Firefly DL | FLIR Systems*. 6.06.2020. URL: https://www.flir.eu/products/firefly-dl/.

[39] *Casia - Iris Automation*. 2.06.2020. URL: https://www.irisonboard.com/casia/.

[40] Victor Castro et al. *Active Noise Cancellation System for UAVs*. 2017.

[41] reichelt elektronik GmbH &amp and Team, Co. KG Internet. *DEBO SEN ULTRA - Entwicklerboards - Ultraschall Abstandssensor, HC-SR04*. 14.06.2020.

[42] Balemir Uragun and I. Tansel. "The noise reduction techniques for Unmanned Air Vehicles". In: *2014 International Conference on Unmanned Aircraft Systems, ICUAS 2014 - Conference Proceedings* (May 2014). DOI: 10.1109/ICUAS.2014.6842325.

[43] D. Miljković. "Methods for attenuation of unmanned aerial vehicle noise". In: *2018 41st International Convention on Information and Communication Technology, Electronics and Microelectronics (MIPRO)*. 2018, pp. 0914–0919.

[44] Hyun D Kim, Aaron T Perry, and Phillip J Ansell. "A review of distributed electric propulsion concepts for air vehicle technology". In: *2018 AIAA/IEEE Electric Aircraft Technologies Symposium (EATS)*. IEEE. 2018, pp. 1–21.

[45] Ohad Gur and Aviv Rosen. "Design of quiet propeller for an electric mini Unmanned air vehicle". In: *Journal of Propulsion and Power* 25.3 (2009), pp. 717–728.

[46] N Kloet, S Watkins, and R Clothier. "Acoustic signature measurement of small multi-rotor unmanned aircraft systems". In: *International Journal of Micro Air Vehicles* 9.1 (2017), pp. 3–14.

[47] Angus Leslie, Kee Choon Wong, and Doug Auld. "Broadband noise reduction on a mini-UAV propeller". In: *14th AIAA/CEAS Aeroacoustics Conference (29th AIAA Aeroacoustics Conference)*. 2008, p. 3069.

[48] Yannian Yang et al. "Experimental study on noise reduction of a wavy multi-copter rotor". In: *Applied Acoustics* 165 (2020), p. 107311.

[49] Igor S Kovalev et al. "'Butterfly acoustical skin'–new method of reducing aero acoustical noise for a quiet propeller". In: *Journal of Engineering Mechanics* 4 (2019), pp. 1–28.

[50] Antonio J Torija, Zhengguang Li, and Rod H Self. "Effects of a hovering unmanned aerial vehicle on urban soundscapes perception". In: *Transportation Research Part D: Transport and Environment* 78 (2020), p. 102195.

[51] S Watkins et al. "Ten questions concerning the use of drones in urban environments". In: *Building and Environment* 167 (2020), p. 106458.

[52] Kyle Pascioni and Stephen A Rizzi. "Tonal Noise Prediction of a Distributed Propulsion Unmanned Aerial Vehicle". In: *2018 AIAA/CEAS Aeroacoustics Conference*. 2018, p. 2951.

[53] Sen M Kuo and Dennis R Morgan. "Active noise control: a tutorial review". In: *Proceedings of the IEEE* 87.6 (1999), pp. 943–973.

[54] Kirk Graham Stewart Cartwright. "Feasibility of parachute recovery systems for small UAVs". In: *The UNSW Canberra at ADFA Journal of Undergraduate Engineering Research* 1.2 (2009), p. 8.

[55] Piotr Bartkowski and Robert Zalewski. "Passive safety system for small unmanned aerial vehicles". In: *MATEC Web of Conferences* 157 (2018), p. 03001. DOI: 10.1051/matecconf/201815703001.

[56] Katarına Draganová, Václav Moucha, and František Kmec. "Safety Equipment and Emergency Procedures for UAV Control". In: *SCIENTIFIC CONFERENCE MODERN SAFETY TECHNOLOGIES IN TRANSPORTATION*. 2013, p. 44.

[57] Alan Jamal Erickson. *Inflatable parachute airbag system*. US Patent 9,611,045. Apr. 2017.

[58] Premium-Modellbau. *T-Motor Antigravity MN5006 450kv Multicopter Brushless Motor 4-6S 106g*. 29.06.2020. URL: https://www.premium-modellbau.de/t-motor-antigravity-mn5006-450kv-multicopter-brushless-motor-4-6s-106g.

[59] *Flugmodell Brushless Elektromotor A20-22 L EVO Hacker kV (U/min pro Volt): 924 Windungen (Turns): 22 kaufen*. 29.06.2020. URL: https://www.conrad.de/de/p/flugmodell-brushless-elektromotor-a20-22-l-evo-hacker-kv-u-min-pro-volt-924-windungen-turns-208758.html.

[60] Patrick Leiner. *Drohnen selber bauen tunen: Ohne Vorkenntnisse: Drohne, Quadrocopter, Multicopter: Schritt für Schritt selbst gebaut*. 1. Aufl. Modellbau. s.l.: Franzis, 2016. ISBN: 3645604448. URL: http://gbv.eblib.com/patron/FullRecord.aspx?p=4688786.

[61] Dave Deptula and Eric Mathewson. *Air Force Unmanned Aerial System (UAS) Flight Plan 2009-2047*. Tech. rep. Air Force Washington DC Director Intelligence Surveillance and Reconnaissance, 2009.

[62] *DIN EN ISO 12100 (2011-03-00) - General principles for design - Risk assessment and risk reduction*.

[63] Francesco Cocchioni, Adriano Mancini, and Sauro Longhi. "Autonomous navigation, landing and recharge of a quadrotor using artificial vision". In: *International Conference on Unmanned Aircraft Systems (ICUAS), 2014*. Piscataway, NJ: IEEE, 2014, pp. 418–429. ISBN: 978-1-4799-2376-2. DOI: 10.1109/ICUAS.2014.6842282.

[64] Lee Ferrell. "How To Get Approval to Fly BVLOS-Part 107". In: (). URL: https://www.faa.gov/uas/resources/events_calendar/archive/2019_uas_symposium/media/How_To_Get_Approval_to_Fly_BVLOS-Part_107.pdf.

[65] Press. "FAA approves another groundbreaking BVLOS flight". In: *sUAS News* (15.8.2019). URL: https://www.suasnews.com/2019/08/faa-approves-another-groundbreaking-bvlos-flight/.

[66] EASA. "Opinion No 05-2019". In: (). URL: https://www.easa.europa.eu/sites/default/files/dfu/Opinion%20No%2005-2019.pdf.

[67] EASA. "EASA Opinion No 01/2020". In: (). URL: https://www.easa.europa.eu/sites/default/files/dfu/Opinion%20No%2001-2020.pdf.

[68] vdiv. "DHL fliegt Medikamente mit Drohne auf die Nordseeinsel Juist". In: *ingenieur.de - Jobbörse und Nachrichtenportal für Ingenieure* (25.9.2014). URL: https://www.ingenieur.de/technik/fachbereiche/verkehr/dhl-fliegt-medikamente-drohne-nordseeinsel-juist/.

[69] Jake Bright. "Zipline begins US medical delivery with drone program honed in Africa". In: *TechCrunch* (27.5.2020).

[70] Heinrich-Hertz-Institut, Fraunhofer. *Call a drone: Controlling drones via voice channels – Fraunhofer Heinrich Hertz Institute*. 6.06.2020. URL: https://www.hhi.fraunhofer.de/en/press-media/news/2018/call-a-drone-controlling-drones-via-voice-channels.html.

[71] Michaela Sankowsky. "„Aktionsplan Drohnen" des BMVI". In: *droniq-store* (15.5.2020). URL: https://droniq.de/blogs/news/aktionsplan-drohnen-des-bmvi?_pos=1&_sid=84aa11534&_ss=r.

[72] Frederic Lardinois. "A first look at Amazon's new delivery drone". In: *TechCrunch* (5.6.2019). URL: https://techcrunch.com/2019/06/05/a-first-look-at-amazons-new-delivery-drone/.

[73] *Ready to Fly - Aerotenna*. 6.11.2017. URL: https://aerotenna.com/readytofly/.

[74] *Pixhawk 2.1 Standard & Here 2 GNSS Set*. 6.06.2020. URL: https://www.robotshop.com/de/en/pixhawk-21-standard--here-2-gnss-set.html.

[75] David Lee Hall, James Llinas, and Martin E. Liggins, eds. *Handbook of multisensor data fusion: Theory and practice*. Second edition. The electrical engineering and applied signal processing series. Boca Raton, FL: CRC Press, 2009. ISBN: 9781420053081. URL: http://proquest.tech.safaribooksonline.de/9781351835374.

[76] G. Migliaccio, G. Mengali, R. Galatolo. "Conflict detection and resolution algorithms for UAVs collision avoidance". In: *The Aeronautical Journal* 118.1205 (2014), pp. 828–842.

[77] Cesar A. Munoz et al. "A Family of Well-Clear Boundary Models for the Integration of UAS in the NAS". In: (2014). URL: https://ntrs.nasa.gov/search.jsp?R=20150000558.

[78] Joram Verstraeten, Martijn Stuip, and Tom van Birgelen. "Assessment of Detect and Avoid Solutions for Use of Unmanned Aircraft Systems in Nonsegregated Airspace". In: *Handbook of unmanned aerial vehicles*. Ed. by Kimon P. Valavanis and George J. Vachtsevanos. Dordrecht: Springer, 2015, pp. 1955–1979. DOI: 10.1007/978-90-481-9707-1{\textunderscore}70.

[79] *FLARM*. 10.07.2020. URL: https://flarm.com/.

[80] *Radar for navigation support of autonomous flying drones - Fraunhofer FHR*. 6.06.2020. URL: https://www.fhr.fraunhofer.de/en/press-media/press-releases/2018/radar_for_navigation_support_from_autonomous_flying_drones.html.

[81] *mSharp Patch Collision Avoidance Radar Introduction Package - Aerotenna*. 17.12.2018. URL: https://aerotenna.com/shop/%ce%bcsharp-patch/.

[82] He Zhang, Vishwanath Sindagi, and Vishal M. Patel. "Image De-raining Using a Conditional Generative Adversarial Network". In: *IEEE Transactions on Circuits and Systems for Video Technology* (2019), p. 1. ISSN: 1051-8215. DOI: 10.1109/TCSVT.2019.2920407.

[83] *Detection of small drones with millimeter wave radar*. 6.06.2020. URL: https://www.fhr.fraunhofer.de/en/businessunits/security/Detection-of-small-drones-with-millimeter-wave-radar.html.

[84] Anthony Narkawicz, Aaron Dutle, and George Hagen. *DAIDALUS: Detect and Avoid Alerting Logic for Unmanned Systems*. 2015.

[85] Maria Consiglio et al. "ICAROUS: Integrated configurable algorithms for reliable operations of unmanned systems". In: *35th DASC - Digital Avionics Systems Conference*. Piscataway, NJ: IEEE, 2016, pp. 1–5.

[86] Swee Balachandran et al. "A Learning-Based Guidance Selection Mechanism for a Formally Verified Sense and Avoid Algorithm". In: *2019 IEEE/AIAA 38th Digital Avionics Systems Conference (DASC)*. IEEE, 8.09.2019 - 12.09.2019, pp. 1–6.

[87] Marvin Rausand. *Risk Assessment: Theory, Methods, and Applications*. Statistics in Practice. Hoboken: Wiley, 2013. ISBN: 9780470637647. DOI: 10.1002/9781118281116. URL: http://search.ebscohost.com/login.aspx?direct=true&scope=site&db=nlebk&db=nlabk&AN=597754.

[88] Kambushev K. M. "ANALYSIS OF THE METHOD FOR PREDICTING THE TECHNICAL CONDITION OF AIRCRAFT EQUIPMENT". In: *Trans Motauto World* 2.5 (2017), pp. 178–180. URL: https://stumejournals.com/journals/tm/2017/5/178.

[89] John William Bennett. "Fault tolerant electromechanical actuators for aircraft: Fault tolerant electromechanical actuators for aircraftUR - https://theses.ncl.ac.uk/jspui/handle/10443/990". PhD thesis. Newcastle University.

[90] "Fuel Cell Technologies Office Multi-Year Research, Development, and Demonstration Plan - Section 3.4 Fuel Cells". In: (). URL: https://www.energy.gov/sites/prod/files/2017/05/f34/fcto_myrdd_fuel_cells.pdf.

[91] Wasserstofftechnologie und Elektromobilität Ingenieurbüro für Brennstoffzelle. *Wie sicher sind Wasserstofffahrzeuge?* [Online; Stand 11. Juli 2020]. 2017. URL: https://emcel.com/de/sicherheit-von-wasserstofffahrzeugen/.

[92] autoevolution. *TOYOTA Mirai 2015 - Derzeitig*. [Online; Stand 19. Juni 2020]. 2020. URL: https://www.autoevolution.com/de/autos/toyota-mirai-2015.html#aeng_toyota-mirai-2015-60-kwh-155-hp.

[93] Kai Liu et al. "Materials for lithium-ion battery safety". In: *Science advances* 4.6 (2018), eaas9820.

[94] Zachary P Cano et al. "Batteries and fuel cells for emerging electric vehicle markets". In: *Nature Energy* 3.4 (2018), pp. 279–289.

[95] Sunita Satyapal. "Hydrogen and Fuel Cells Enabled through the US Department of Energy". In: *Meeting Abstracts*. 34. The Electrochemical Society. 2019, pp. 1791–1791.

[96] Sheridan Few et al. "Prospective improvements in cost and cycle life of off-grid lithium-ion battery packs: An analysis informed by expert elicitations". In: *Energy Policy* 114 (2018), pp. 578–590.

[97] MF Saharudin. "Development of tilt-rotor unmanned aerial vehicle (UAV): material selection and structural analysis on wing design". In: *IOP Conference Series: Materials Science and Engineering*. Vol. 15. 2017.

[98] Horst Neubacher and Klaus Wagner. "Bewertung von Autohäusern". In: *Bewertung von Spezialimmobilien*. Springer, 2018, pp. 207–223.

[99] Rainer Dippold. "Distributionszentren des Online-Handels". In: *Bewertung von Spezialimmobilien*. Ed. by Sven Bienert and Klaus Wagner. Wiesbaden: Springer Fachmedien Wiesbaden, 2018, pp. 721–745. ISBN: 978-3-8349-4737-6. DOI: 10.1007/978-3-8349-4738-3{\textunderscore}23.

[100] Sarah Milanzi et al. *Technischer Stand und Flexibilität des Power-to-Gas-Verfahrens*. Tech. rep. 9. Tech. rep. Department of Energy and Resources Management, TU Berlin, 2018.

[101] E Borgogno Mondino and M Gajetti. "Preliminary considerations about costs and potential market of remote sensing from UAV in the Italian viticulture context". In: *European Journal of Remote Sensing* 50.1 (2017), pp. 310–319.

[102] MM Doole, J Ellerbroek, and JM Hoekstra. "Drone delivery: Urban airspace traffic density estimation". In: *8th SESAR Innovation Days, 2018* (2018).

[103] TQ Hua et al. "Technical assessment of compressed hydrogen storage tank systems for automotive applications". In: *International Journal of Hydrogen Energy* 36.4 (2011), pp. 3037–3049.

[104] Statista. *Global electricity prices in 2018, by select country*. 2018. URL: https://www.statista.com/statistics/263492/electricity-prices-in-selected-countries/ (visited on 06/27/2020).

[105] Fitt Small Business. *Drone Insurance: Cost, Coverage Why You Need It*. 2018. URL: https://fitsmallbusiness.com/drone-insurance/ (visited on 06/04/2020).

[106] Travers Aviation. *Drone Insurance Cost*. 2018. URL: https://www.traversaviation.com/drone-insurance-cost.html (visited on 06/04/2020).

[107] eurostat. *Arbeitskosten pro Stunde lagen 2017 in den EU Mitgliedstaaten zwischen 4,9 und 42,5*. 2017. URL: https://ec.europa.eu/eurostat/documents/2995521/8791193/3-09042018-BP-DE.pdf/bcad2022-0fbc-4c21-811d-5fef8399ee5f (visited on 06/23/2020).

[108] EASA. "Introduction of a regulatory framework for the operation of unmanned aircraft". In: (). URL: https://www.easa.europa.eu/sites/default/files/dfu/Introduction%20of%20a%20regulatory%20framework%20for%20the%20operation%20of%20unmanned%20aircraft.pdf.

[109] JARUS. *JARUS guidelines on Specific Operations Risk Assessment (SORA)*. URL: http://jarus-rpas.org/sites/jarus-rpas.org/files/jar_doc_06_jarus_sora_v2.0.pdf.

[110] *Package Delivery by Drone (Part 135)*. 29.06.2020. URL: https://www.faa.gov/uas/advanced_operations/package_delivery_drone/.

[111] *UPS Flight Forward Attains FAA's First Full Approval For Drone Airline*. 29.06.2020. URL: https://pressroom.ups.com/pressroom/ContentDetailsViewer.page?ConceptType=PressReleases&id=1569933965476-404.

[112] *VTOL Aircraft for BVLOS Missions - Avy*. 29.06.2020. URL: https://www.avy.eu/bvlos-vtol-drone-aircraft.

[113] Magyarits and Sherri. *Unmanned Aircraft System (UAS) Traffic Management (UTM)*. URL: https://www.faa.gov/uas/research_development/traffic_management/media/UTM_ConOps_v2.pdf.

[114] *EHang | UAM - EHang's Smart Logistics Ecosystem*. 29.06.2020. URL: https://www.ehang.com/logistics/.

[115] *Voll autonome Lieferdrohne*. 29.06.2020. URL: https://www.qopter.de/de/lieferdrohne.php.

[116] *Technology - Volansi - FLY ANYTHING ANYWHERE*. 1.05.2020. URL: https://volansi.com/technology/.

[117] *Technology – Wingcopter GmbH*. 29.06.2020. URL: https://wingcopter.com/technology.

[118] *African Drone Forum – Transforming mobility through technology*. 29.06.2020. URL: https://www.africandroneforum.org/.

[119] Cooper Smith. "The surprising facts about who shops online and on mobile". In: *Business Insider* February 23 (2015).

[120] Seyed Mahdi Shavarani, Mazyar Ghadiri Nejad, Farhood Rismanchian, and Gokhan Izbirak. "Application of hierarchical facility location problem for optimization of a drone delivery system: a case study of Amazon prime air in the city of San Francisco". In: *The International Journal of Advanced Manufacturing Technology* 95.9-12 (2018), pp. 3141–3153.

[121] Fixlastmile. *6 ways to reduce your last mile delivery costs in your business*. URL: https://www.fixlastmile.com/blog/reduce-last-mile-delivery-costs-in-your-business/ (visited on 06/28/2020).

[122] Roel Gevaers, Eddy Van de Voorde, and Thierry Vanelslander. "Cost modelling and simulation of last-mile characteristics in an innovative B2C supply chain environment with implications on urban areas and cities". In: *Procedia-Social and Behavioral Sciences* 125.2014 (2014), pp. 398–411.

[123] *Pixhawk 2.1 Standard Autopilot*. 29.06.2020. URL: https://www.sgbotic.com/index.php?dispatch=products.view&product_id=2613.